AUTOMATIC SEGMENTATION AND CLASSIFICATION OF PHANTOM IMAGES FOR MAMMOGRAPHY QUALITY CONTROL

M.Sc. THESIS

TEKLEWEYNI BERHE

DECEMBER 2019

HARAMAYA UNIVERSITY, HARAMAYA

Automatic Segmentation and Classification of Phantom Images for Mammography Quality Control

A Thesis Submitted to the Department of Physics,

Postgraduate Programme Diroctorate

HARAMAYA UNIVERSITY

In Partial Fulfillment of the Requirements for the Degree of

MASTER OF SCIENCE IN PHYSICS (COMPUTATIONAL PHYSICS)

Tekleweyni Berhe

December 2019

Haramaya University, Haramaya

HARAMAYA UNIVERSITY

POSTGRADUATE PROGRAMME DIROCTORATE

As thesis advisors, we hereby certify that we have read and evaluated this thesis prepared under our guidance, by **Tekleweyni Berhe** entitled: **"Automatic Segmentation and Classification of Phantom Images for Mammography Quality Control ".** We recommend that it be submitted as fitting the thesis requirement.

Getachew Abebe (PhD)	__________	____________
Major Advisor	Signature	Date
Seife Teferi (PhD)	__________	____________
Co-Advisor	Signature	Date

As members of the Board Examiners of the Final M.Sc.Thesis Open Defense, we certify that we have read and evaluated the thesis prepared by **Tekleweyni Berhe** and examined the candidate. We recommend that the thesis be accepted as fulfilling the Thesis requirement for the degree of Master of Science in Physics (Computational Physics).

______________	__________	____________
Chairperson	Signature	Date
______________	__________	____________
Internal Examiner	Signature	Date
______________	__________	____________
External Examiner	Signature	Date
______________	__________	____________
Director, Postgraduate Programme Directorate	Signature	Date

Final approval and acceptance of the Thesis is contingent upon the submission of its final copy to the Council of Postgraduate Programs Directorate (CPGPD) through the candidate's department or Post Graduate Committee (DGC or PGC).

DEDICATION

I dedicate this thesis to my beloved family for their consistent and unreserved encouragement throughout my educational carriers.

STATEMENT OF THE AUTHOR

By my signature below, I declare and affirm that this thesis is my own work. I have followed all ethical and technical principles of scholarship in the preparation, data collection, data analysis and compilation of this thesis. Any scholarly matter that is included in the thesis has been given recognition through citation.

This thesis is submitted in partial fulfillment of the requirements for M.Sc. degree at Haramaya University. The Thesis is deposited in the Haramaya University Library and is made available to borrowers under rules of the Library. I solemnly declare that this Thesis has not been submitted to any other institution anywhere for the award of any academic degree, diploma or certificate.

Brief quotations from this Thesis may be made without special permission provided that accurate and complete acknowledgement of source is made. Requests for permission for extended quotation from or reproduction of this Thesis in whole or in part may be granted by the Head of the Department of Physics or the Director of postgraduate Directorate when in his/her judgment the proposed use of the material is in the interests of scholarship. In all other instances, however, permission must be obtained from the author of the Thesis.

Name: Tekleweyni Berhe Signature: __________________

Date: ________________

School/Department: Physics

BIOGRAPHICAL SKETCH OF THE AUTHOR

The author, Mr. Tekleweyni Berhe was born to his father Berhe Beyene and mother Zimam Abay, in Centeral Zone at T/michew Woreda, Tigray Regional State, North Ethiopia in 1990 G.C. He attended his junior school at Kewanit primary school and his secondary and preparatory education at Wukro Maray senior secondary and preparatory school in Axum.

Upon successful completion of his preparatory school, he joined Mekelle University in 2010/2011 and graduated in a Bachelor of Science degree in Applied Physics on July 06, 2013 G.C. After his graduation he was employed by the Ministry of Education at Chelenko Senior Secondary and Preparatory School as Physics teacher. While he was serving as a physics teacher, he joined Haramaya University in summer program and graduated with a Postgraduate Diploma in Teaching (PGDT) on October 08, 2014 G.C. After serving as Physics teacher for one year at Chelenko, he was employed and served for two years at Haramaya University Model school and then as senior technical Assistant at Haramaya University for one year and 6 months. While he was serving at the later position in 2017/2018 G.C he joined Postgraduate program Directorate at Haramaya University to pursue his Master of Science in Physics (Computational Physics).

ACKNOWLEDGEMENTS

Above all, the author is grateful to Almighty God for his love and kindness and for bestowing him health, strength, patience and protection throughout his postgraduate studies and thesis preparation. The author extends his deepest gratitude to Getachew Abebe (PhD) his Major Advisor, for his lovely and ever-unforgettable warm welcome at his office, adding valuable comments, always provide advice, patiently supervising, guiding and assisting in the course of the thesis work, and Seife Teferi (PhD) his Co-Advisor, giving directions, suggestions and moral encouragement starting from the inception to the accomplishment of the study.

The author is thankful to the Ethiopian Ministry of Education (MoE) for financing the research work. He is also grateful to the Postgraduate Program Directorate of Haramaya University and College of Natural and Computational Sciences for hosting him and for all rounded services during the study period, and Physics Department, for unlimited support in printing materials.

The author's thank also goes to Kadisco General Hospital and technicians who gave him technical supports during mammogram and phantom reading and interpretation.

He also takes this opportunity to give deep thanks to his friends Tsigabu G/mariam, Dejenie Demissie and staff members for their help and encouraging to accomplish this work.

His special thanks and heartfelt gratitude extend to his mother Zimam Abay, brothers, and sister, his wife Saron Tegegne and his daughter Arsema Tekleweyni and all his other family members and all his friends for their incredible moral supports.

ACRONYMS AND ABBREVIATIONS

AC	Accuracy
ACR	American College of Radiology
ANN	Artificial Neural Network
BC	Breast Cancer
CAD	Computer Aided Detection
CC	Cranio-Caudal
CLAHE	Contrast Limited Adaptive Histogram Equalization
DIP	Digital Image Processing
FN	False Negative
FP	False Positive
IQ	Image Quality
MATLAB	Matrix Laboratory
MCCs	Micro Calcification
MLO	Medio-Lateral Oblique
QA	Quality Assurance
QC	Quality Control
RoI	Region of Interest
SE	Sensitivity
SP	Specificity
TN	True Negative
TP	True Positive
WHO	World Health Organization

TABLE OF CONTENTS

TABLE OF CONTENT (CONTINUED)

LIST OF TABLES

Table **Page**

LIST OF FIGURES

LIST OF TABLES IN THE APPENDIX

LIST OF FIGURES IN THE APPENDIX

Appendix Figures **Page**

Automatic Segmentation and Classification of Phantom Images for Mammography Quality Control

ABSTRACT

Breast cancer is one of the most common forms of cancer in women worldwide. At present, mammography is one of the most reliable methods for early breast cancer detection. However, mammography images are difficult to interpret by the experts owing to the fact their features are typically very small, have poor contrast and a wide range of anatomical patterns. In order to evaluate the quality of the mammographic facilities, the visibility and the scoring of features in phantom image is used. The goal of this research was to automate breast phantom image scoring using image processing techniques. First breast phantom films were digitized. For each category of structures, sub-images were extracted from the digitized phantom. Artifacts were removed using extraction process and noise was removed by the 2D median filter. Contrast-limited adaptive histogram equalization (CLAHE) algorithm was used to improve the appearance of the image. The morphological features of the phantom images were also calculated. Ten digitized phantom images were extracted into sub-images and 150 sample sub images were considered for the evaluation. Artificial Neural Network (ANN) was used as classifiers. For each classifier, the performance factor such as sensitivity, specificity and accuracy are computed. All the techniques were implemented through MATLAB R2013a platform. It is observed that the proposed scheme with ANN classifier out performed by giving 96% accuracy, 95% sensitivity, 92.5% specificity and 4% the probability of misclassification error to classify the phantom images as fiber, specks or mass.

Keywords: ANN, CLAHE, GLCM, Mammography, Phantom, Quality control, Segmentation.

1. INTRODUCTION

1.1. Background of the Study

Breast cancer is the uncontrolled growth of cells in the breast region, and it is the second leading cause of cancer deaths in women today (Pradeep *et al*., 2012). Similarly in Ethiopia, breast cancer is the second most often occurring cancer among women (semarya *et al.,* 2013). According to World Health Organization (WHO), breast cancer is the most common cancer in women both in the developed and the developing countries. Moreover, there is an increasing incidence of breast cancer in the developing world because of the increase in life expectancy, urbanization and adoption of western lifestyles. However, early detection of the cancer can reduce mortality rate. Early detection of breast cancer can be achieved using digital mammography, typically through detection of characteristic masses and micro-calcifications. A mass is defined as a space-occupying lesion seen in at least two different projections. Masses are described by their shape and margin characteristics. Calcifications are tiny calcium deposits within the breast tissue, which appear as small white spots on the mammography film.

There are several imaging techniques for examining the breast, including mammography, ultrasound, magnetic resonance imaging etc. Mammography is the most common breast screening technology. It is a low dose X-ray procedure that allows the visualization of internal structure of the breast and is one of the imaging modality in early breast cancer detection typically through visualization of characteristic masses and micro calcifications. Visualization and detection of cancer cells in mammography play a crucial role in reducing the rate of mortality from breast cancer.

One of the challenges in mammography is low contrast in mammogram images. This poses difficulties for radiologists to interpret the results. Mammography is technically one of the most demanding radiographic investigations though it is difficult to obtain consistently high quality mammograms, due to insufficient contrast between normal and abnormal breast tissue. Poor quality films can only lead to wrong diagnoses and consequently increase the number of inappropriate biopsies. To be effective, mammography requires a quality assurance mechanism to produce high-quality images, ensure patient safety, and provide timely treatment. Quality assurance(QA) mechanism is one of the recipes in any working environment which aims to ensure the result of a working procedure meets some predefine quality standard. Quality Control (QC) shows the performance of the mammography system as it degrades in time, However, the aim is always to attain the highest image quality, which the mammographic X-ray machine can deliver. In order to maintain high image quality and learn that it is not deteriorate over a long period of time, it is usual to take and evaluate one or more phantom's images for monitoring its quality at regular intervals (Faulkner and Law, 1994).

There are many advantages in using phantoms for the evaluation of the mammographic images quality. One of them is to test the visibility of objects distributed in their body constitution, setting the best image in order to obtain a safe medical diagnostic, and optimizing the risk/benefit ratio to the patient. Currently, the quality of the mammographic image is estimated by performing subjective and quantitative assessments (Leitz *et al.*, 1993). As a subjective evaluation, the technique of visual grading analysis (VGA), consists of clinical direct observation of radiographic images (Perry *et al*., 2008). The success of this evaluation depends on the parameters involved in the process of professional formation, on the skill of the observer and also on the quality of auxiliary equipment's such as light source, resolution of the computer screen and printing system (Mayo *et al.*, 2004). The quantitative analysis can be performed on the phantom images for the test objects. These objects are specially designed to simulate conditions in case of breast cancer, or to allow the determination of image resolution (Mayo *et al.*, 2004).

The phantom is considered as the representation of human breast containing its major components as fat, glandular and connective tissues. It has also masses, fibers and micro calcifications that might be seen in the breast developing cancer. Accurate identification of these features in the mammographic images attributed to the quality of the X-ray machine in addition to the skill of the radiographers. The use of phantom may be considered as a tool to monitor the quality of X-ray machine. This work is aiming at developing objective technique to identify the masses, fibers and micro calcifications of mammographic images of phantom.

1.2. Statements of the Problem

Breast cancer is the leading cause of cancer mortality among middle aged women. However, early detection of breast cancer increases the survival rate and also the treatment options.

Currently, screening mammography is the most effective tool for early detection of breast cancer. However, the relevance of the diagnosis is highly correlated with the quality of the mammographic system. Reading mammography image is a very demanding job and difficult to interpret by experts or radiologists because the features are very small, poor contrast and have a wide range of anatomical patterns. This makes the detection and diagnosis difficult. While screening the patient by X-ray device some problems such as the patient exposure to high radiation dose may occur and this does not comply with the standard of radiation protection that lead to the patient's future problem. These problems are due to the high kilovoltage parameter (kVp) and tube current (mAs). Hence periodic monitoring of mammographic facilities is required in order to ensure that they work properly. This can be done by evaluating the image quality of a mammographic phantom film. This phantom is intended to be used as an integral part of the mammographic quality control program, and when used in routine mammographic QC, it helps in easily, and accurating evaluates the overall imaging performance of mammographic system.

1.3. Objective of the Study

1.3.1. General objective

The general objective of this study is to automate breast phantom scoring using image processing techniques.

1.3.2. Specific objectives

The specific objectives of this study are:

- To segment important structures such as masses, micro calcification and fibers.
- To extract morphological features of the test objects.
- To classify features using Artificial Neural Network.
- To verify the performance of the classifier.

1.4. Scope of the Study

This work focuses on evaluation of the QC of mammographic imaging system using reference phantoms by processing its digitized image. The digital image processing and analysis provide information about the phantom characteristics which are not easily obtained by means of direct observation of the image. Information about the test objects allow characterizations of the phantom image obtained and using these parameters, the status of the imaging system could be determined. The small size and the low contrast of the test objects make them difficult to be seen by observers. So, it is important to establish some visibility criteria for the different test objects, which can be analyzed automatically, and in approximately the same way as can be done by an expert (medical physicist or radiologists), which provides reproducible quantitative results.

1.5. Significance of the Study

Currently, there are no effective ways to prevent breast cancer, because its cause remains unknown. Therefore, urgency and importance of mammography image processing is obvious. Computer-Aided Detection (CADe) and Computer-Aided Diagno-sis (CADx) systems are continuously being developed aiming to help the physicians in early detection of breast cancer. Computer-Aided Diagnosis can improve the detection of early stage malignancy. However, improvements still need to be done in order to decrease the risk of developing cancer to the minimal. Automating this score by using computer image processing of digitized phantom films could make the evaluation of mammographic facilities easier and less subjective. In addition, image processing enables us to take into account other parameters such as, noise, and shape of the targets that a reader eye cannot estimate quantitatively, and to perform a more elaborated analysis.

The need for monitoring quality of mammography imaging system is well documented (Payne and Lawinski, 1992). As the result, phantoms are used to assess image quality, equipment performance and reduce patient exposure. Imaging of test phantoms provides information about the performance of the system in terms of measurable physical parameters such as high and low contrast resolution.

There are multiple advantages in using phantoms for image quality evaluation. Firstly, the test objects that constitute the phantom and their distribution are known and unvarying for a given phantom. Secondly, images of the phantom under non-clinical conditions can be obtained without the involvement of (exposing) the patient. Finally, it is possible to obtain as many phantom images as necessary for inter-comparison, thus allowing the study of image quality over an extended period (Mayo *et al.,* 2004). This work may help radiologist in clinical decision for quick, easy, and accurate evaluation of the overall imaging performance of mammographic system.

2. LITERATURE REVIEW

2.1. Mammography

Mammography is the screening process that uses low-energy X-rays to examine a woman's breast. The X-ray image makes it possible to detect tumors, which cannot be felt by patients. Currently, there are two kinds of mammograms, screening and diagnostic mammograms. The screening mammogram is used to check for breast cancer in women who have no signs or symptoms of the disease. The diagnostic mammogram is used to check for breast cancer after a lump or other symptom of the disease has been found. Besides a lump, signs of breast cancer can include breast pain, thickening of the breast skin, nipple discharge, and a change in breast size or shape. However, these signs may also be signs of benign disease symptoms. Digital mammograms take an electronic image of the breast and store it directly in a computer. Breast abnormalities that can indicate cancer are masses, calcifications, architectural distortions and bilateral asymmetry (Vaidehi and Subhashini, 2012). A sample mammogram displaying the female breast anatomy is shown in Figure 2.1.

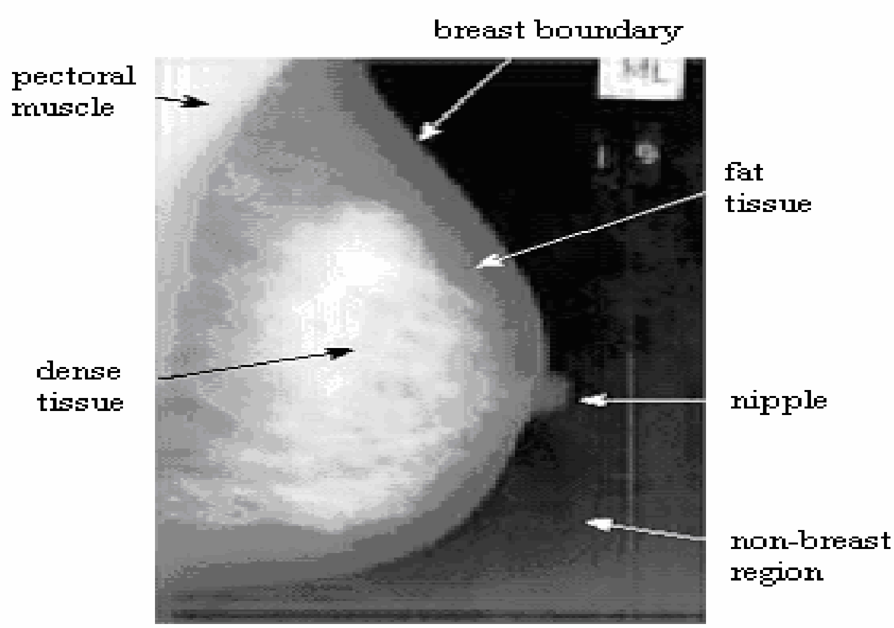

Figure 2.1. Mammographic of Female Breast Anatomy (Laine and Huda, 1996).

The requirements for mammography are high contrast, high spatial resolution, and minimal radiation exposure. High contrast is needed because differences in density between normal and pathologic structures of the breast tissue are small.

In mammographic screening, each breast is imaged separately with two views: the Medio-Lateral Oblique (MLO) view and the Cranio-Caudal (CC) view. Figure 2.2 (a) shows the two viewpoints of X-rays. Figures b) and c) show two example mammograms of each view. For the same breast, each view is intended to show different appearances and details of breast tissue. For instance, the R symbol which appears in Figure 2.2 is used to mark the mammogram as right breast.

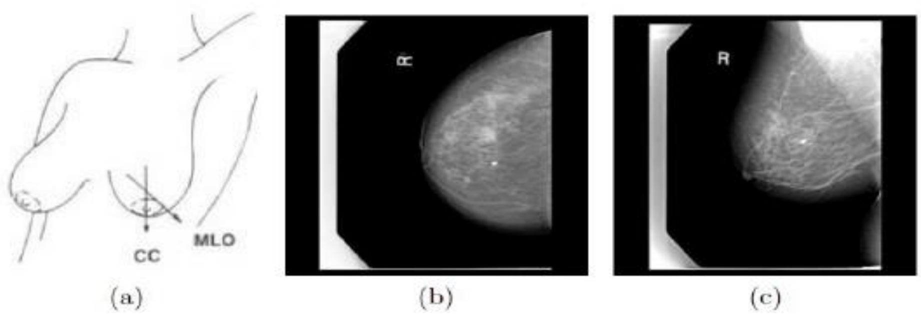

Figure 2.2. Different viewpoints of mammogram (Laine and Huda, 1996). **a**) The direction of the two viewpoints, **b**) The media-lateral oblique view and **c**) The crania-caudal view.

To acquire a woman breast image, the patient stands in front of a mammography machine, and one of her breasts is placed on a clear plastic plate gently but firmly pressed from another plate above her breast. The plates flatten the breast and keep it still, which helps produce a better mammogram image. The pressure lasts a few seconds and does not harm the breast. Experienced radiologists can carefully compress the breasts to improve the view without rupturing the implant. These procedures are undertaken in order to capture good quality mammographic image. However, the quality of the image is also complicated by the film type and machine configuration parameters such as voltage and exposure, and with X-ray scatter and noise.

2.2. Mammography Image Quality Control

In the case of medical imaging, the image used as a means to get information of the health status of the patient, and ultimately, image quality in various diagnostic tasks should be measured by evaluating the impact of the image in carrying correct diagnosis (ICRU, 1996). This has proven to be difficult. Establishing the link between physical image quality measures and clinical utility has been pursued for decades (Wanger *et al*., 2001). Mammography image quality (IQ) refers to the level of detail information offered by a particular X-ray system configuration, which allows for the recognition of relevant features in a breast image (Lawrence *et al.*, 2004). The analysis of the IQ obtained from a mammography phantom of reference is one of the main points in a complete quality control program of mammography equipment (Fischmann *et al*., 2005). In many applications, including medical imaging, image quality can be reasonably defined in relation with the performance of the image in transmitting information.

Quality control is a diagnostic procedure, it covers monitoring, evaluation, and maintenance at optimum levels of all characteristics of performance that can be defined, measured, and controlled. Quality control is the cornerstone of practicing high image quality mammography. To ensure high quality, the ACR has established a voluntary program for the accreditation of mammographic screening sites (Kimme *et al*., 1992). Such QC system must be implemented to monitor the proper functioning of elements such as X-ray equipment, radiographic films development conditions, digital system etc involved in the mammography image processing. Appropriate functioning of all systems in the process produces a good quality mammography image which can help to carry out a suitable diagnosis with minor possible radiation dose. The measurement of the quality of the images provides evidence about the quality processing procedures. In the ACR phantom image evaluation, the entire mammographic imaging chain as the set represents one quality control measurement required for accreditation. The evaluation involves the analysis of a test phantom that consists of the objects that simulate masses in the breast.

2.3. Phantom and Test Objects Description

Phantom is a specially designed object that is scanned or imaged in the field of medical imaging to evaluate, analyze, and tune the performance of various imaging devices. The phantom used in this study is the ACR phantom (Model–156), Phantom Serial Number: 1103074). The ACR Phantom is the standard phantom for the Mammography Quality Standards Act (MQSA) and ACR quality control programs. It estimates the radiation dose delivered to patient and evaluate the quality of the image. A phantom is more readily available and provides more consistent results than the use of a living subject or cadaver, and likewise avoids subjecting a living subject to direct risk. Phantoms were originally employed for use in 2D X-ray based imaging techniques such as radiography or fluoroscopy. A phantom image is used to perform quality control in mammographic facilities. The interpretation of the ACR phantom images depends upon the experience, visual threshold, scoring criteria and state of the observer. Radiograph of a phantom are taken to assess image density, contrast, and uniformity, mass, speck groups, and fibres in the phantom. There exist various types of reference phantoms, the fundamental differences are the number of test objects and complexity. The phantom reference used in this work is commercialised by the ACR firm of Model–156 reference. The phantom is used to detect small structures that are important in the early detection of breast cancer. Figure 2.3 shows an ACR phantom.

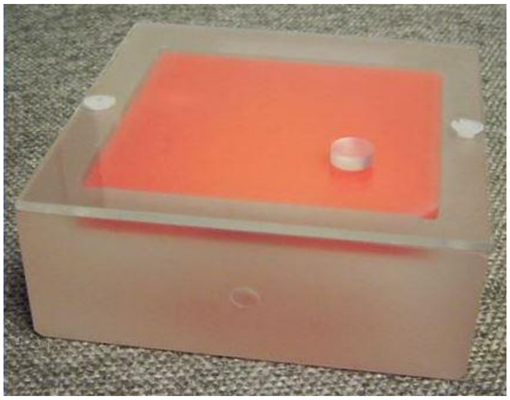

Figure 2.3. American College of Radiology (ACR) Phantom

Figure 2.3, shows the phantom is made of a 7 mm wax block insert containing 16 sets of test objects, a 3.4 cm thick acrylic base, and a 3 mm thick cover.

Acrylic refers to a synthetic resin or textile fibres made from polymers of acrylic acid or acrylates. The phantom approximates a 4.0 – 4.5 cm compressed breast of average glandular (connective tissue)/adipose (fatty tissue) composition. All the test objects are contained in a wax block which is enclosed in an acrylic base. Materials used to simulate test objects are nylon fibers or fishing lines used as fibers; aluminum oxide particles marble stone chips, and epoxy resin(a solid or liquid synthetic organic polymer used as the basis of plastics, adhesives) as masses; $CaCO_3$ or bone are used as specks(Possible sources of $CaCO_3$ are chicken eggs, ostrich egg, marble stone, sea shells and chalks).

Table 2.1 Physical characteristics of ACR Phantom.

Characteristics	ACR Phantom
Overall thickness	4.4 cm
Wax block thickness	7 mm
Acrylic base thickness	3.4 cm
Cover thickness	3 mm
Composition	4.5 cm compressed breast of average glandular/adipose composition
Number of inserted objects	
Fibers (Diameter, mm)	6 (1.56, 1.12, 0.89, 0.75, 0.54, 0.40)
Specks (Diameter, mm)	5 (0.54, 0.40, 0.32, 0.24, 0.16)
Masses (Diameter, mm)	5 (2.00, 1.00, 0.75, 0.50, 0.25)

The ACR phantom is used as a standard measure of the image chain performance of mammography systems (Haus *et al.*, 1993). Figure 2.4 shows structures of the phantom with six fibers, five speck groups, and five masses. Initially, the test objects (artefacts) and their approximate locations are defined. The shapes include: six rectangular shaped nylon fibres slanted at ±45° to simulate soft tissue edges, five groups with six spherical specks of aluminium oxide in each group to simulate micro-calcifications (specks) and five larger lens shape water density masses to simulate tumours. Figure 2.4 shows structures of the phantom with six fibers, five speck groups and five masses.

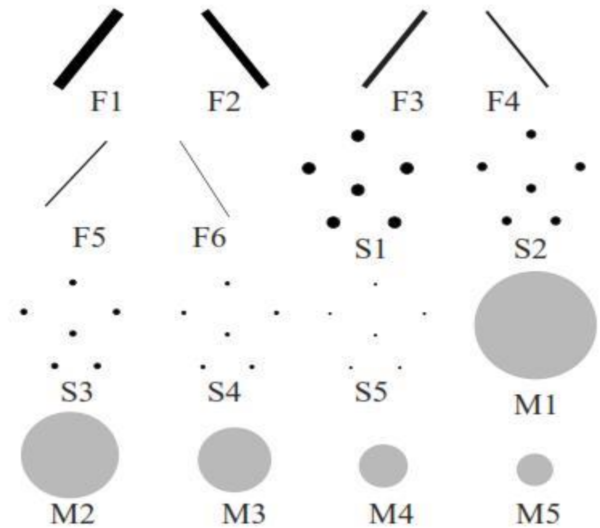

Figure 2.4. Radiograph of the ACR phantom showing the light grey, fibres (F1, F2, F3, F4, F5, F6), specks group (S1, S2, S3, S4, S5), and masses (M1, M2, M3, M4, M5).

The ACR phantom has 6 fibers with diameters of 1.56 (F1), 1.12 (F2), 0.89 (F3), 0.75 (F4), 0.54 (F5), and 0.40 mm (F6) mm; 5 speck groups with 6 specks in each group, with speck diameters of 0.54 (S1), 0.40 (S2), 0.32 (S3), 0.24 (S4), and 0.16 mm (S5) mm; and 5 masses with decreasing diameters and thickness of 22.00 (M1), 1.00 (M2), 0.75 (M3), 0.50 (M4), and 0.25 mm (M5), respectively.

Table 2.2. Description of the ACR phantom (RMI-156).

Label	Diameter (mm)	Label	Diameter (mm)	Label	Thickness (mm)
F1	1.56	S1	0.54	M1	2.00
F2	1.12	S2	0.40	M2	1.00
F3	0.89	S3	0.32	M3	0.75
F4	0.75	S4	0.24	M4	0.50
F5	0.54	S5	0.16	M5	0.25
F6	0.40	-	-	-	-

As shown in Table 2.2, the test objects within the phantom range in size from those that should be visible on any system to objects that are difficult to see even on the best mammographic systems.

These test objects are constructed so that their visibility in the resultant mammographic images ranges from the easily visible to the invisible, and, therefore, these objects straddle the threshold of visibility (Huda *et al.*, 2002). The X-ray image of the ACR phantom should permit visualization of the largest four fibrils, three speck groups with the largest specks and largest three masses. Under standard testing procedures, the average number of objects detected in each group (masses, specks and fibrils) should not changed by more than 50% if viewed under ideal conditions by the same observer. The small size and weight of the ACR phantom makes it convenient to mail between the institution and the analysis site (Chakraborty, 1997). The depiction of these objects in mammographic images is usually scored by qualified medical physicists (Haus *et al.*, 2001).

2.4. Digital Image Processing

Image can be defined as a two-dimensional function f(x, y), where x and y are spatial coordinates and f is the intensity or gray-level of the image at the point. When x, y, and intensity value of f are all finite discrete quantities, we call the image a digital image. Digital image processing refers to processing a digital image by means of digital computer. There is a fundamental step in DIP; image acquisition, image enhancement, morphological processing, segmentation, representation and description, and recognition (Gonzalez and Wood, 2008).

2.4.1 Median filter

The median filter is a nonlinear (a filter whose output is not a linear function of its input) digital filtering technique, often used to remove noise while it preserves edges. Such noise reduction is a typical pre-processing step to improve the results of the subsequent processing (edge detection on an image, for instance). It is one of the best windowing operators out of the many windowing operators like the mean filter (Boateng *et al*., 2012). The median filter filters each pixel in the image in turn and its nearby neighbors are used to decide whether or not it is representative of its surroundings. Normally, instead of replacing the pixel value with the mean of neighboring pixel values, median filter replaces it with the median of those values. That is, the values from the surrounding neighborhood are first sorted into numerical order, and then the value of the pixel in question is replaced with the middle (median) pixel value.

The neighborhood is referred to as the window. The window can have various shapes centered on the target pixel. The square is a typical shape to be chosen for windows defined for 2D images. It should be noted that under normal circumstances the median filter, is performed using a window containing an odd number of pixels. If the neighbourhood under consideration consists of an even number of pixels, the median value selected as the output is the average of the two middle pixel values.

2.4.2. Enhancement

Image enhancement techniques are used to improve an image, where improvement is sometimes defined objectively (example increase the signal-to-noise ratio), and sometimes subjectively (example make certain features easier to see by modifying the colors or image's intensity values to a new range) (Singh *et al*., 2011). In this research, the phantom image was enhanced using contrast limited adaptive histogram equalization (CLAHE).

Contrast limited adaptive histogram equalization is an adaptive image contrast enhancement technique based on histogram modification, and it operates on small regions (blocks) in an image and improves the local contrast of the image. CLAHE is used to limit the appearance of an artifacts and noise, a modification of histogram equalization (HE) called contrast limited adaptive HE. Contrast limited adaptive histogram equalization method seeks to reduce the noise produced in homogeneous areas and was originally developed for medical imaging (Khuzi *et al*., 2009). Ordinary histogram equalization uses the same transformation derived from the image histogram to transform all pixels. Likewise adaptive histogram equalization has a tendency to over amplify noise (that is, the random fluctuation of image signals) in relatively homogeneous regions of an image. A variant of adaptive histogram equalization called contrast limited adaptive histogram equalization (CLAHE) prevents this problem by limiting the amplification. However, CLAHE has a tendency to over amplify noise in relatively homogeneous regions of an image. Contrast limited adaptive histogram equalization differs from ordinary histogram equalization in the respect that the adaptive method computes several histograms, each corresponding to a distinct section of the image, in its contrast limiting, and uses them to redistribute the lightness values of the image. It is used to prevent the over amplification of noise came by adaptive histogram equalization (Sharma, 2013).

Algorithm of CLAHE (Sharma, 2013):

1. Obtain all the inputs: Image, Number of regions in row and column directions, Number of bins for the histograms used in building image transform function (dynamic range), Clip limit for contrast limiting (normalized from 0 to 1).
2. Pre-process the inputs: Determine real clip limit from the normalized value if necessary, pad the image before splitting it into regions.
3. Process each contextual region (tile) thus producing gray level mappings: Extract a single image region, make a histogram for this region using the specified number of bins, clip the histogram using clip limit, and create a mapping (transformation function) for this region.
4. Interpolate gray level mappings in order to assemble final CLAHE image: Extract cluster of four neighbouring mapping functions, process image region partly overlapping each of the mapping tiles, extract a single pixel, apply four mappings to that pixel, and interpolate between the results to obtain the output pixel.

2.4.3. Thresholding

Thresholding is the simplest image segmentation method. Thresholding process converts a multilevel image into a binary image. There are different types of thresholding techniques. If a single threshold is used for the whole image, it is called global thresholding. If the threshold varies over the image and depends on local characteristics of sub-images, it is called local thresholding. This method divides an original image into several sub regions, and chooses various thresholds T for each sub region. It can be determined interactively based on an operator's visual assessment of the segmentation result. On the other hand, there are many automatic threshold selection methods. Specifically Otsu’s method is a type of global thresholding which depends only on gray value of the image. Otsu’s thresholding is widely used because it is simple and effective and requires computing a gray level histogram before running. In this study, otus’s thresholding was used to segmente the artifacts (mass, fiber and specks) of the phantom images. Otsu algorithm can obtain satisfactory segmentation results when it applied to the noisy images. Otsu’s method was one of the better threshold selection methods for general real world images with regard to uniformity and shape measures (Vala and Baxi, 2013).

Otsu set the threshold so as to try to minimize the overlapping of the class distributions. Otsu's thresholding method corresponds to the linear discriminant criteria that assumes that the image consists of only object (foreground) and background, and the heterogeneity and diversity of the background is ignored (Otsu, 1979). Otsu set the threshold so as to try to minimize the overlapping of the class distributions (Otsu, 1979). Given this definition, the Otsu's method segments the image into two, light and dark regions T_0 and T_1 respectively. Where region T_0 is a set of intensity level from zero to t or in set notation $T_0 = \{0, 1, \ldots, t\}$ and region $T_1 = \{t, t+1, \ldots, l-1, l\}$ where t is the threshold value, l is the image maximum gray level. T_0 and T_1 can be assigned to object and background or vice versa (object not necessarily always occupies the bright region). Otsu's thresholding method scans all the possible thresholding values and calculates the minimum value for the pixel levels each side of the threshold. Otsu's method determines the threshold value based on the statistical information of the image where for a chosen threshold value t the variance of clusters T_0 and T_1 can be computed.

2.4.4. Morphological operators

Morphology is a broad set of image processing techniques that process images based on shapes. Morphological operations apply using a structuring element to an input image, creating an output image of the same size. In a morphological operation, the value of each pixel in the output image is based on a comparison of the corresponding pixel in the input image with its neighbors. The most basic morphological operations are dilation and erosion.

2.4.4.1. Binary image dilation and erosion

Dilation adds pixels to the boundaries of objects in an image, while erosion removes pixels on object boundaries. Dilation causes objects to dilate or grow in size. If A is a binary image and B the structuring element, dilation of A by B, denoted, A⊕ B is defined as

$$A \oplus B = \{Z \mid (B)_Z \cap A \neq \emptyset\} \tag{2.1}$$

This equation is based on obtaining the reflection of B denoted as B about its origin and shif ting the reflection by z. The dilation of A by B then, the set of all displacements, z, such that B and A overlap by at least one element as

$$A \oplus B = \{z|(B)_z \cap A \subseteq A\} \tag{2.2}$$

$$D\,(A, B) = A \oplus B\ U_{d \in b}\ (\{c + d|c \in\ a\}) \tag{2.3}$$

This operation is implemented by successively placing the centre pixel of the structuring elem ent on each background pixel, if any of the neighbourhood pixels are foreground pixels, then the background pixel is switched to foreground. An application of dilation is bridging gaps in binary images, that is, filling unwanted holes (backgrounds) surrounded by a foreg round region. The technique can also be used to enlarge an image (Gonzaliz and wood, 2008). Let A to represent a binary image and B the structuring element, then the erosion of A by B, denoted as A⊖B, is defined as

$$A \ominus B = \{z|B_z| \subseteq A\} \tag{2.4}$$

$$E\,(A, B) = A \ominus B\ U_{E\ \in b}\ (\{c - d|c \in\ a\}) \tag{2.5}$$

This equation is implemented by successively placing the centre pixel of the structuring elem ent on each foreground pixel. If any of the neighbouring pixels are background pixels, th en the foreground pixel is switched to background pixel. One simple application of erosion is elimination of irrelevant details (in terms of size) from a binary image.

2.4.4.2. Opening and closing

Opening is the name given to the morphological operation of erosion followed by dilation with the same structuring element. The opening of A by structuring element B as AoB, and is defined as

$$A \circ B = (A \ominus B) \oplus B \tag{2.6}$$

The general effect of opening is removal of small isolated objects from the foreground of an im age,placing them in the background. It tends to smooth the contour of binary objects and break narrow joining regions in an object (Solomon *et al*., 2010). Closing is morphological operation of dilation followed by erosion with the same structuring element. The closing of A by B is denoted as A● B, and is defined as

$$A \bullet B = (A \oplus B) \ominus B \tag{2.7}$$

Closing tends to remove small holes in the foreground, changing small regions of background in to foreground (Solomon *et al*., 2010).

2.4.5. Morphological features

Morphological image feature is used to represent shape, size and boundary regions of objects of the image. Shape and size of characteristics of phantom images information can be analyzed and used for several operations depending on the purpose of this work. The algorithm was develop to extract the following morphological feature data from images:

i. Area (A): of a test object was measured by counting the number of pixels inside the region covered by test objects having a value of 1.

ii. Major Axis Length (Major): is the distance between the end points of the longest line that could be drawn through the test objects. The major axis end points are found by computing the pixel distance between every combination of border pixels in the test objects (mass, fiber and micro calcification) boundary and finding the pair with the maximum length.

iii. Minor Axis Length (Minor): is the distance between the end points of the longest line that could be drawn through the test objects (mass, fiber and micro calcification) while maintaining perpendicularity with the major axis.

iv. Aspect Ratio (Elongation): is ratio of the length of the major axis to the length of the minor axis.

$$Elongation = \frac{\text{Major}}{\text{Minor}} \text{ or } \frac{\text{Length}}{\text{width}} \tag{2.8}$$

V. Orientation: The angle (in degrees ranging from -90 to 90 degrees) between the x-axis and the major axis of the ellipse that has the same second-moments as the region.

Vi. Perimeter: The distance around the boundary of the region.

Vii. Circularity ratio: The ratio of the area of a shape to the area of a circle having the same perimeter.

$$Circularity\ ratio = \frac{\text{Area of Shape}}{\text{Area of bounding circle}} \tag{2.9}$$

2.5. Artificial Neural Networks

An Artificial Neural Network (ANN) is an information processing model that is stimulated by the way biological nervous systems, such as the brain, process information. An Artificial Neural Network is configured for a specific application, such as pattern recognition or data classification, through a learning process.

Artificial Neural Network collective behavior is characterized by their ability to learn recall and generalize training patterns or data similar to that of a human brain. The features that can be used as training data include, shape, size of nodule, granularity and morphological feature. These features can be extracted manually or using image analysis technique. In this work, multilayer feed forward neural networks using back propagation algorithm. This is the most widely used neural network model and its design consists of one input layer, one hidden layer, and one output layer. Each layer is made up of non-linear processing units called the neurons, and the connections between neurons in successive layers carry associated weight or features. Connections are directed and allowed only in the forward direction, e.g. from input to hidden, or from hidden layer to an output layer. Back-propagation is agradient-descent algorithm (an optimization algorithm used to minimize some function by iteratively moving in the direction of steepest descent as defined by the negative of the gradient) that minimizes the error between the output of the training input or output pairs and the actual network output (Fausett, 1994).

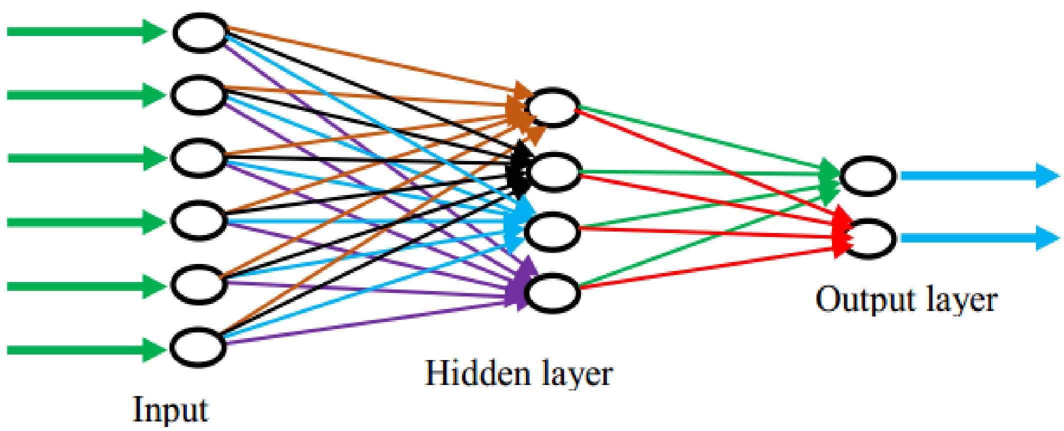

Figure 2.5. Structure of the multi-layer neural network.

Using the above feature vector representations, a neural classifier was trained and tested to recognize and classify the phantom images. To train the network, the input and target data need to be fed into the network. The extracted image features were used as input and the test obiects of each selected phantom images considered in this study gave to the target data. The network then divided the input data into three different data sets, which are training, validation and testing samples. The training data are used to train the network and the network is adjusted according to its error.

3. MATERIALS AND METHODS

3.1. Sampling Techniques

In this study, the mammography of ACR accredited phantom was used as the standard for verification. Ten samples of phantom images were collected from Kadisco General Hospital in Addis Ababa/ Ethiopia. Then, a set of image processing algorithms was developed to quantitatively analyze each of the different artifacts found in the ACR phantom, with three radiologists, who indicate the number of masses, specks and fibers visible in each image. The radiologist chooses the tube voltage of the best phantom image for each at different kv and then the algorithm applied to the image to determine the maximum number of visible masses, specks and fibers and compare with the radiologists' evaluation of the phantom images. Each phantom area (artifacts) in the ACR phantom requires a specific algorithm. A set of digitized ACR phantom images were processed by the algorithms for detection and scoring features. The results then compared to the radiologist's scores for each test object in the phantom images. Three experienced radiologic technologists assessed all of the phantom images and then conferred and decided scores for each test object in the phantom images. The assessments were performed using the film.

For this research work, computer, mammography image of phantom and MATLAB Software to implement all image processing and analysis algorithms have been used.

3.2. Film Acquisition and Digitalization

The ACR phantom was placed on X-ray machine and imaged using different tube voltage/current values. In total ten ACR phantom images were captured and scored by three experienced radiologists. The experts indicated the number of masses, specks and fibers visible in each image. The radiographs were then scanned with high resolution drum scanner (Model EU-22, # 015129) producing images of maximum size, 2018 × 2028 pixel*s*, and a grey scale resolution of 8 bits/pixel with spatial resolution of 600 dpi (dot per inch), that is to say, the dynamic range of gray level intensity had 256 different values and saved in an image file using JPEG (Joint Photographic Experts Group) format. Each phantom image differed from other phantom image in their kV values.

The voltage tube and tube current was varied between 25 and 34kVp, 49.7mAs and 92 mAs respectively. Then, the images were pre-processed and treated using various techniques such as filtering, image segmentation using thresholding, morphological operations, etc.

3.3. Image Processing and Analysis

The methodlogy used for automatic segmentation and classification of phantom image consists of the following stages i.e. preprocessing, segmentation, feature extraction and classification. MATLAB R2013a image processing toolbox was used for image pre-processing, features extraction classification and verification of the performance. Figure 3.1 shows the flowchart of the steps applied to preprocess, segment, extract and classify features of mammographic phantom images.

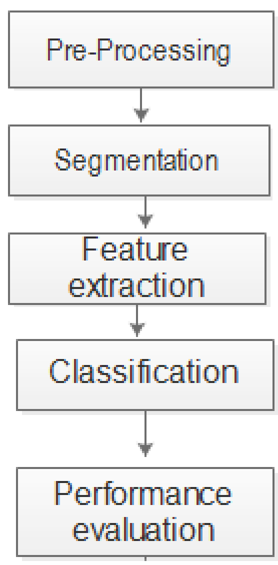

Figure 3.1. Flow chart of the image processing steps applied to phantom images.

3.3.1. Image pre-processing

Usually the images obtained were suitable for straight away identification and classification purpose due to the possible adulteration of noise due to lighting variability, poor resolutions of images, unwanted background, etc. Image pre-processing provides the techniques to enhance the images for further analysis. It also serves for removing an irrelevant part of the foreground and improves the quality of image.

Pre-processing is further used for binarization the mammographic phantom image. In this study, the images were filtered using median filter. Then after, each test objects were enhanced by CLAHE, which was suitable for improving the contrast of the image by operating on small regions (blocks) in an image.

3.3.2. Image segmentation

Image segmentation is the process of partitioning a digital image into multiple segments (sets of pixels, also known as super-pixels). Segmentation of the pixels is usually based on certain similarity criteria such as grey level intensity, color, shape and so on. There are several types of segmentation algorithms that are available today and the performance of these algorithms is goal specific. Thresholding creates binary images from grey-level ones by turning all pixels below the thresholding value to zero and all pixels above the thresholding value to one. A complete segmentation of an image R is a finite set of regions R_1, • • • Rs,

$$R = \bigcup_{i=1}^{s} R_i\,, \qquad R_i \cap R_j = \emptyset, \quad for \;\; i \neq j \tag{3.1}$$

Complete segmentation can result from thresholding in simple scenes. Thresholding is the transformation of an input image f to an output (segmented) binary image G as follows:

$$G(i,j) = \begin{cases} 1 & \text{if } f(i,j) \geq T \\ 0 & \text{otherwise} \end{cases} \tag{3.2}$$

where, T is the threshold value, G(i, j) = 1 for image elements of objects and G(i, j) = 0 for image elements of the background. Otsu’s thresholding operation automatically chooses the pixels that make the object of interest as the foreground pixels and the rest as background pixels. Given the distribution of gray-level in a given image certain gray-level value can be chosen as threshold value that separates the pixels into groups. In a simple case, a single threshold value T is chosen. All the pixels whose gray level value is greater than or equal to T become foreground and all the rest become background pixels.

3.3.3. Classification and verification

Classification is the final stage of determination of artifacts (in our case, the phantom images classified as mass, fiber and specks) recognition using the morphological features.

In this thesis work, the classification is carried out using artificial neural network. This classifier is often work based on characteristic features of a given abnormality such as mass, micro calcification and fibers extracted from phantom mammographic images. As shown in the Figure 3.2, test objects classification using ANN includes input layer, hidden and output layer. The morphological features were used as an input to the ANN based classifier. The classification process is divided into the training and the testing phases. In the training phase, known data are given to train the classifier. In testing phase, unseen data were used to evaluate the performance of the trained classifier (Verma and Zhang, 2007). Figure 3.2 shows the MATLAB structure of Neural Network.

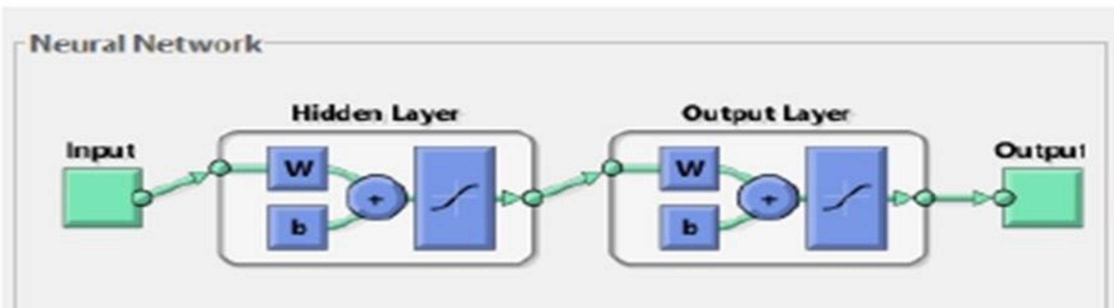

Figure 3.2. MATLAB structure of Neural Network.

3.3.4. Performance measurement

Three performance measurement items, Accuracy (AC), Sensitivity (SE) and Specificity (SP) were used to evaluate the performance of the classifier. Sensitivity is a proportion of positive cases that are well detected by the test. Specificity is a proportion of negative cases that are well detected by the test (it focuses on the test objects detected by radiologist but not the algorithm). Classification accuracy depends on the number of samples correctly classified. The three are defined as follows:

$$\mathrm{AC} = \frac{\mathrm{TP} + \mathrm{TN}}{\mathrm{TP} + \mathrm{FP} + \mathrm{TN} + \mathrm{FN}} \times 100\% \qquad (3.3)$$

$$\mathrm{SP} = \frac{\mathrm{TN}}{\mathrm{TN} + \mathrm{FP}} \times 100\% \qquad (3.4)$$

$$\mathrm{SE} = \frac{\mathrm{TP}}{\mathrm{TP} + \mathrm{FN}} \times 100\% \qquad (3.5)$$

Where, TP is the number of true positives; FP, the number of false positives; TN, the number of true negatives and FN, the number of false negatives.

4. RESULTS AND DISCUSSION

This Chapter presents the results and discussion obtained from different methodologies implemented. All the techniques were implemented using MATLAB R2013a platform.

4.1. Digitizing of Phantom Images

Ten phantom images were collected from the same mammography units and standard mammography films under different clinical conditions. All of the radiographs were digitized using a laser film digitizer. Figure 4.1 shows the digitized phantom images of the first experiment with a matrix size of 256×256 pixels.

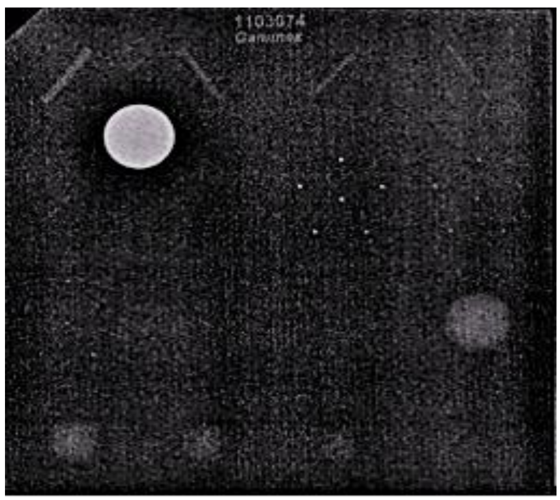

Figure 4. 1. Digitalized phantom image.

4.2. Segmentation of the Region of Interest

In this step the phantom images were manually cropped into sub-images centered on objects of interest containing clusters of fibers, specks and masses. From each phantom image, four sub images containing objects of interest were cropped. There were two main reasons that led us to take this choice. First, expert readers could not detect more than four objects on the phantoms used in this study, secondly, a mammographic facility is considered to produce good quality phantom films if at least four objects are detected for each embedded target. The same resolution 256×256 was used for size comparison of the test objects. Figure 4.2 shows an example of sub images cropped from a digitized phantom film.

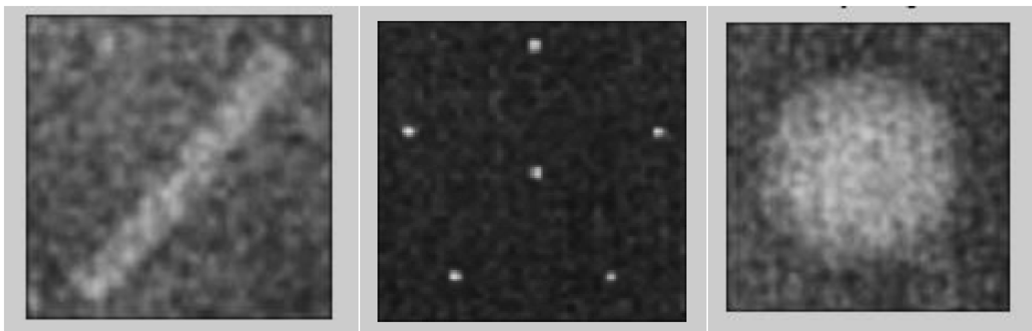

. (a) (b) (c)

Figure 4.2. Sub images segmented for region of interest from a digitized phantom film. (a) fibers (F1), (b) specks and (c) Mass(M1).

4.3. Phantom Image Processing

In this study, first RGB sub artifact images were converted into intensity images using the MATLAB builtin function rgb2gray. The gray intensity image converted is clearly shown in Figure 4.3.

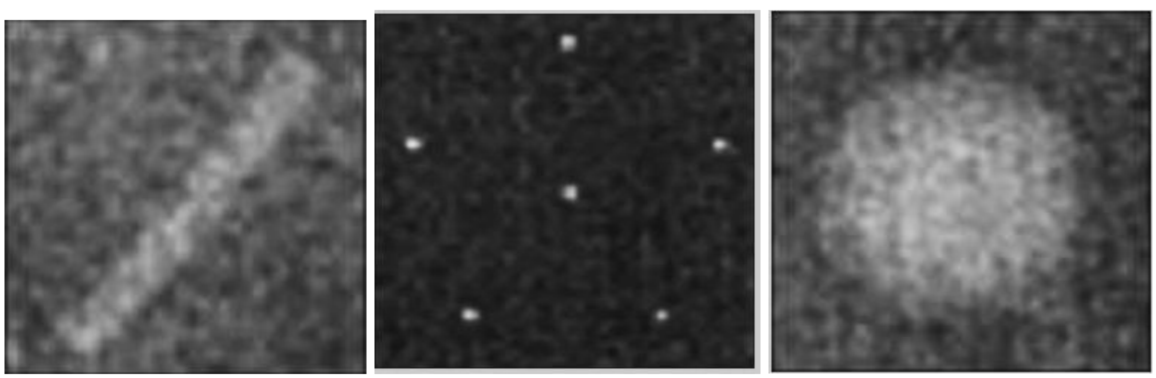

. (a) (b) (c)

Figure 4.3. Gray scale orginal artifact images. (a) fiber (F1), (b) speck (S1) and (c) Mass (M1).

After converting the rgb images into gray images, the next task is employing contrast enhancement technique using histogram modification, that operates on small regions (blocks) in an image to improve the local contrast of the image. For all phantom images, the contrast enhancement limit was set in the range of (0 up to 1) as higher values result in image distortion, which precludes the further detection of region of interest.

In this work, CLAHE method of enhancement was applied to the phantom images only to easily identify the mass, specks and fibers after removal of small area objects. As shown in Figure 4.4, the contrast of gray scale artifact image was enhanced by adaptive HE technique. A MATLAB builtin function adapthisteq was applied to the image in Figure 4.3, with value of 0.01 clip limit which specifies a limit of contrast enhancement, and Rayleigh (Bell-shaped histogram) for distribution which specifies the desired histogram shape for the image. The adapthisteq function is used to perform the operation with a contrast limit (range 0 to 1), which on the overall (normalized) increase in contrast applied to any given region. The result of enhanced artifact images is shown in Figure 4.4, and its MATLAB Function code that has been implemented are clearly illustrated in Appendices (a).

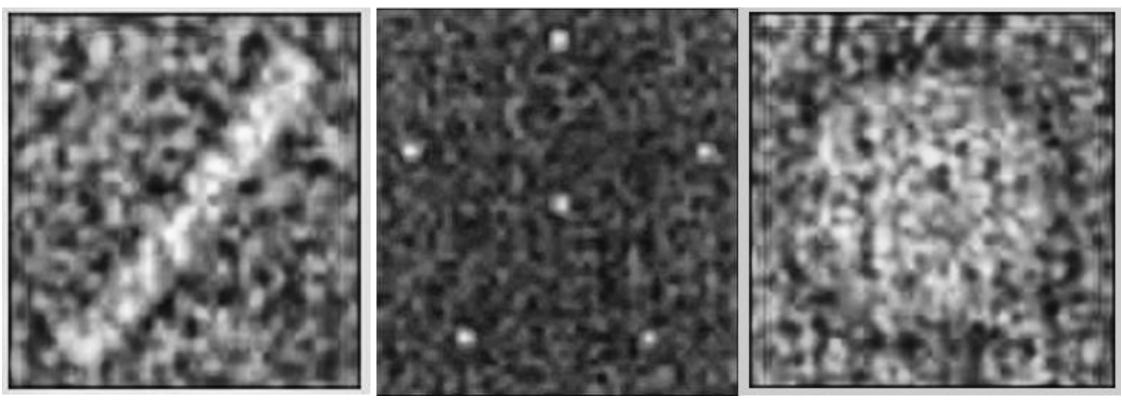

(a) (b) (c)

Figure 4.4. Result of enhanced fiber, speck and mass image using CLAHE. (a) enhanced fiber image, (b) Specks and (c) Mass.

Next, median filter in two dimensions was applied using a MATLAB builtin function medfilt2 with $3x3$ neighborhood size to the contrast enhanced image in order to remove noise or unwanted object within it without affecting the phantom image using 2-D median filter as shown in Figure 4.5.

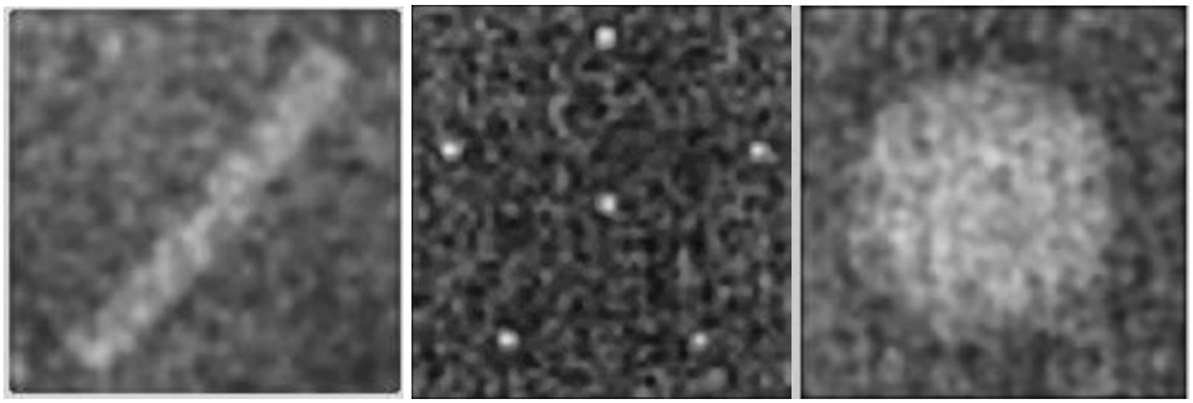

(a) (b) (c)

Figure 4.5. Result of filtered artifact images using median filter. (a) filtered fiber (F1), (b) filtered specks (S1), and (c) filtered mass (M1).

4.4. Segmentation of Phantom Image

The overall results of phantom image segmentation are shown in Figure (4.6, 4.7, and 4.8). Image preprocessing (image enhancement and median filter), segmentation step was followed by steps of image segmentation. In this section, the preprocessed mass, fiber and specks images were automatically segmented using graythresh MATLAB builtin function. This graythresh is an automatic threshold selection region based segmentation method. The histogram gray-level were obtained through MATLAB built in function imhist. Histograms of the grayscale image group pixels value nearby levels to count number of pixels having that level for each gray level. The results of segmented image of each artifact are shown in Figure (4.6, 4.7, and 4.8).

As shown in Figure 4.6 (b), the threshold value T = 50, was determined from histogram of gray image of speck using the MATLAB builtin function imhist. All pixels with gray level value greater than or equal to T were considered as foreground and all pixels out of this bound were considered as background. The result of segmented speck image using Otsu's thresholding is shown in Figure 4.6 (c). Then, this image was opened with morphological bwareaopen operation applied on it in order to remove unwanted small area as shown in Figure 4.6 (d). The imdilate was used to fill holes of the object or foreground of specks. Figure 4.6 (e), which shows a clear dot shape of the specks image.

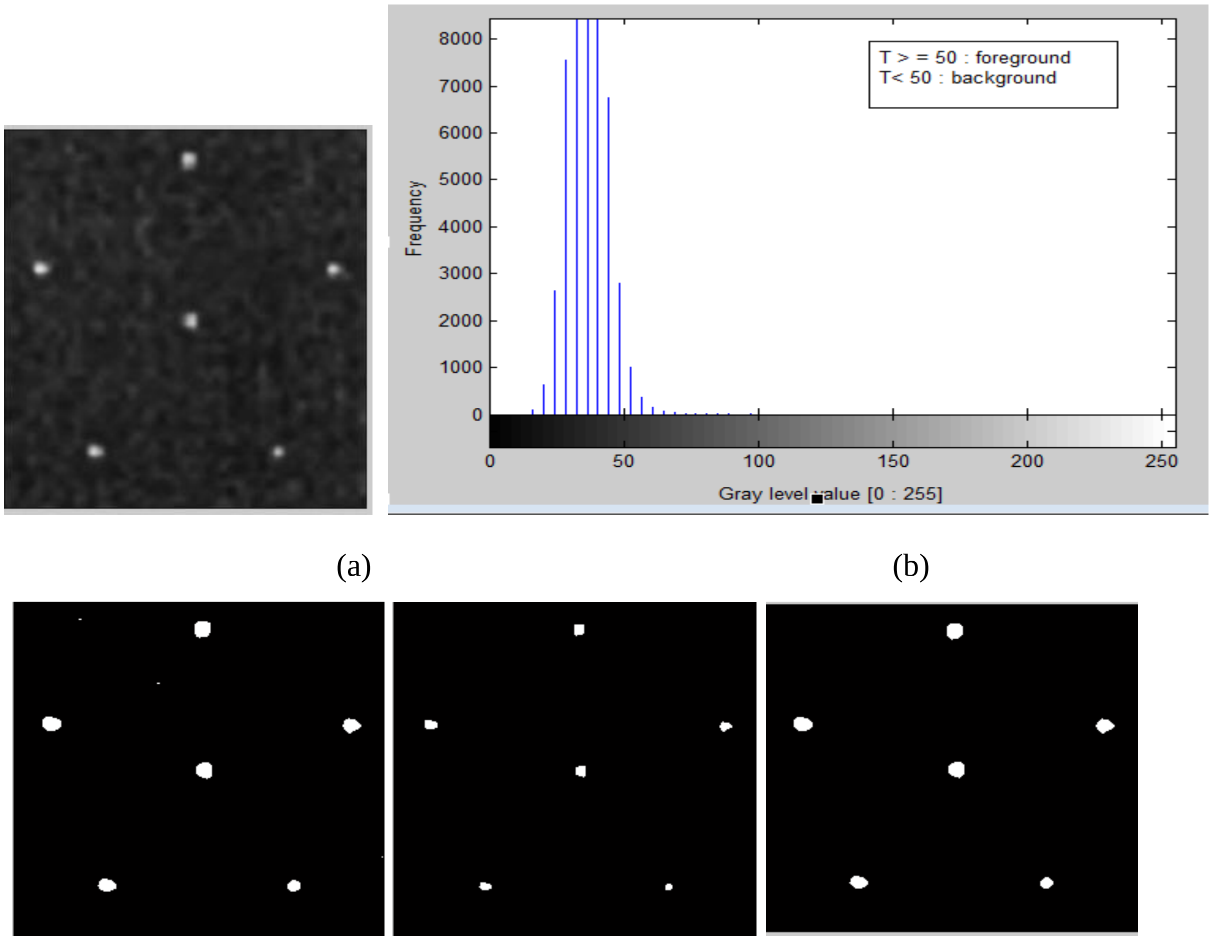

(a) (b)

(c) (d) (e)

Figure 4.6. Segmented specks image. (a) gray scale (S1); (b) histogram gray scale image (S1); (c) segmented (S1); (d) bwareaopen and (e) dilated specks(S1).

The threshold value T = 147, was obtained from histogram of gray image of fiber as shown in Figure 4.7 (b), which automatically segmented the fiber image. All pixels with gray level value greater than or equal to T were considered as object of fiber and all pixels less than the threshloding value T = 147, were considered as background of the fiber. The result of segmented fiber image using Otsu's thresholding is shown in Figure 4.7 (c). This image was opened with morphological (bwareaopen) operation applied on it in order to remove unwanted small area as shown in Figure 4.7 (d). Finally, imdilate operation was used to fill holes of the object or foreground of the fibers. The result of segmented fiber image is shown in Figure 4.7.

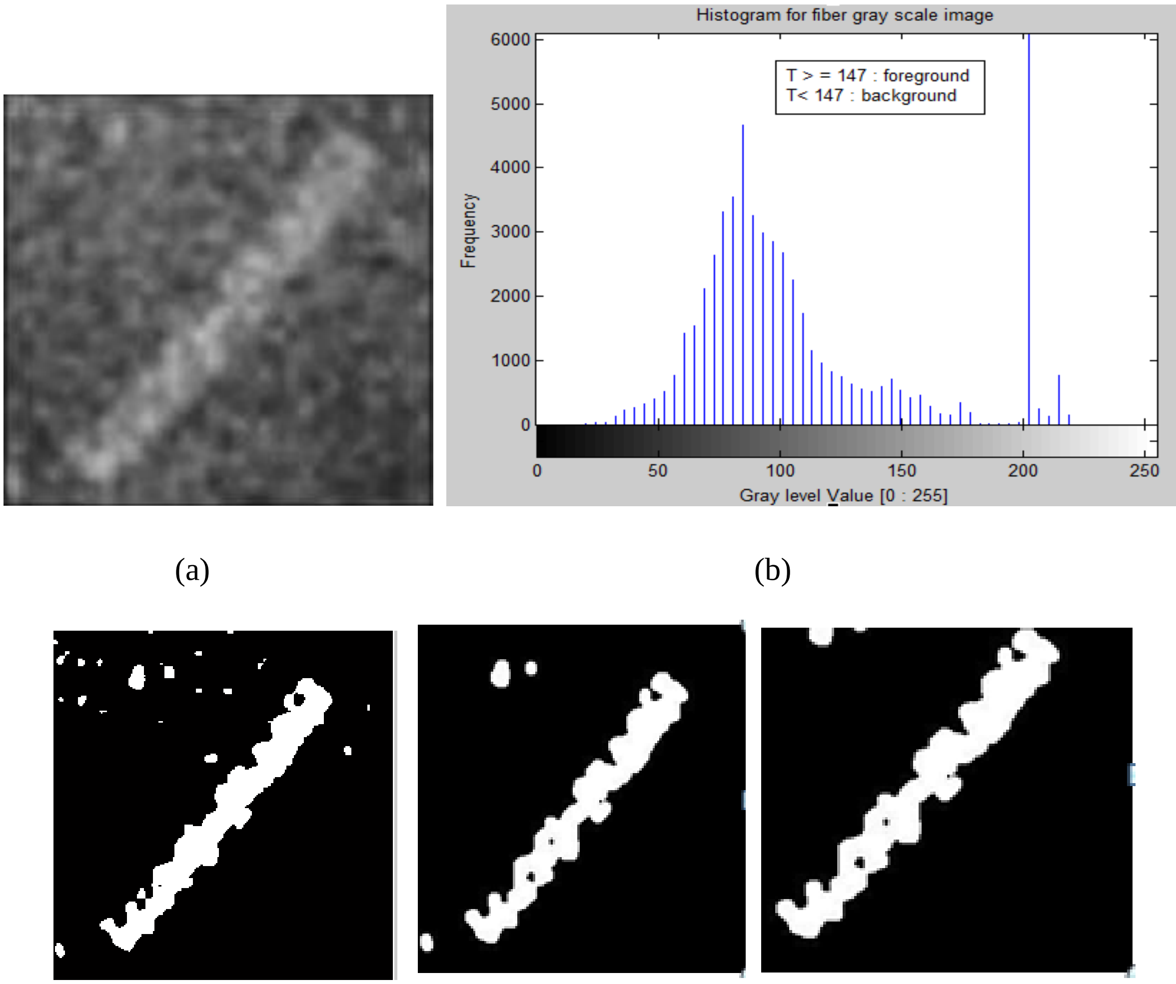

(a) (b)

(c) (d) (e)

Figure 4.7. Segmented fiber images. (a) gray scale (F1); (b) histogram for gray scale image (F1); c) segmented (F1); (d) bwareaopen and (e) dilated fiber(F1).

Figure 4.8 (b), shows that the threshold value T = 104 determined from histogram of gray image of mass. Figure 4.8 (c), shows that all pixels with gray level value greater than or equal to T = 104, were considered as object and all pixels out of this bound were considered as background. The image in Figure 4.8 (d) was opened with morphological bwareaopen operation applied on it in order to remove unwanted small area. Then, the MATLAB command imdilate was used to fill holes of the object or foreground of the mass. the result of segmented mass image as a circle shape is shown in Figure 4.8 (e). The MATLAB code that was used for segmentation of all artifacts using thresholding is annexed in Appendices (e).

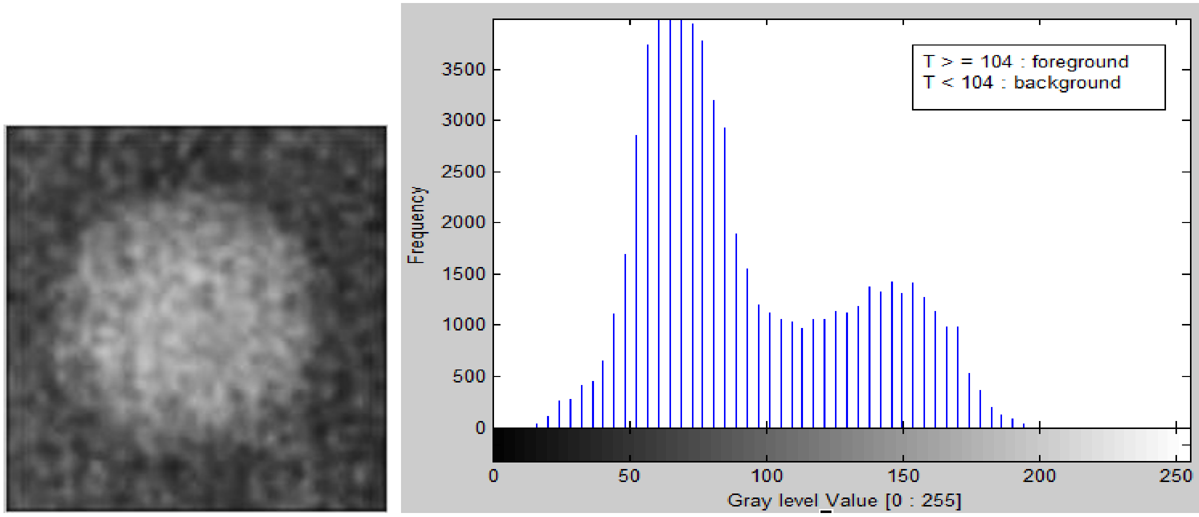

(a) (b)

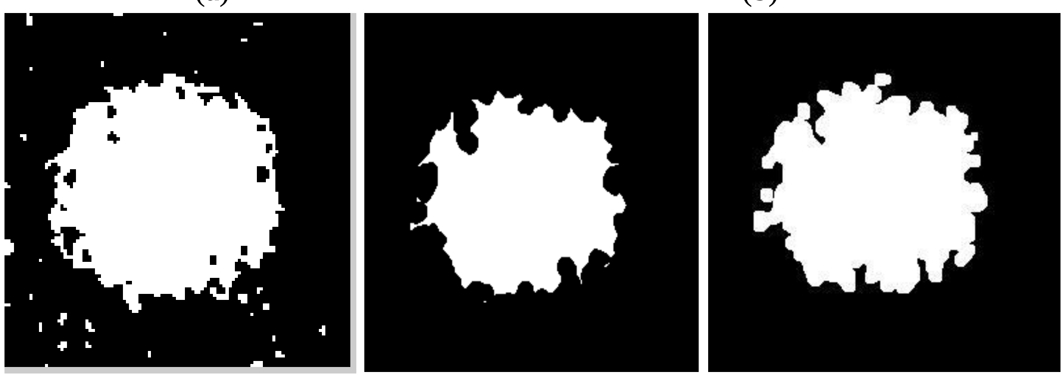

(c) (d) (e)

Figure 4.8. Segmented mass image. (a) gray scale (M1), (b) histogram for gray scale image (M1), c) segmented (M1), (d) bwareaopen and (e) dilated specks (M1).

4.5. Feature Extraction

After segmentation, the step of features extraction is performed by computing morphological features for each artifact (mass, fibers and speck) images. The morphological features such as area, aspect ratio, perimeter, major axis, minor axis, and circularity were extracted using the MATLAB command regionprops, which allowed measuring the properties of phantom images (mass, fiber and speck).

4.5.1. Morphological features

In this study, morphological features such as area, major axis length, minor axis length perimeter, circularity, and aspect ratio were extracted. However, out of these features, area, circularity and elongation were the main morphological components considered to classify the mass, fibers and specks. The results of morphological features of the artifact is shown in Table 4.1.

Table 4.1. Morphological features of masses, fibers and specks of the sample images.

Objects	Area	Major axis	Minor axis	Perimeter	Aspect ratio	Circularity
M1	516	430.59	426.29	29.79	1.04	2.35
F1	1046	378.06	224.72	8.24	1.68	54
S1	304	321.76	295.05	65.49	1.09	1.15
S2	373	227.56	435.05	2.14	0.523	0.95
mm	276	262.71	127.14	43.69	0.98	1.56
mm2	269	345.71	332.74	20.83	1.04	1.32
Fff	301	1.15	1.15	47.36	1	36
Fll	101	132	163.00	52.00	2.98	24
Ss	652	1.15	1.16	2.83	1.00	1.01

Table 4.1. shows that the masses (M1, mm, mm2) and specks (S1, S2, ss) has less circularity than fiber (F1, fff, fll), which indicates that mass and specks are bigger and circular. Furthermore, the elongation value of fibers is further from one, but the elongation value for specks and mass is close to one, which results in a clear dot shape of the specks image and the mass image as a circle/sphere shape.

4.6. Phantom Image Classifications

After the completion of morphological features extraction, the next step is classification of test objects (mass,fiber and specks). The classification was carried out using artificial neural network.

ANN was used to classify test object based on morphological features of the objects in the images. Multilayer feed forward neural networks have been the preferred neural network architectures for the solution of classification and functions approximation problems due to their outstanding learning and generalization abilities (Gong *et al*., 2012).

The main steps in images classification model are three. These are features extraction from each test object images, training the network and test the performance of the network. Accordingly, M, F and S represents data sets for Mass, Fiber and Speck samples respectively. Six selected morphological features were used as input with 20 hidden neurons to get the desired output classification result. The output layer produced either [1 0 0] (mass), [0 1 0] (fiber) or [0 0 1] (specks).

After network setting and input data is ready, the input vector (six features of 150 artifact sample images) and target vector (ground truth of each 150 artifact images, mass, fiber and specks) were divided. Out of 150 artifact images 70% (104 images) were used for training. This process determined the best set of biases for our data set. Only 15% (23 images) were used to validate the network, generalizing and to stop training before over fitting (over fitting happened when the training was good but the testing was bad). The last 15% (23 images) were used as test of the network generalization. The standard network that was used for pattern recognition is shown in Figure 4.9.

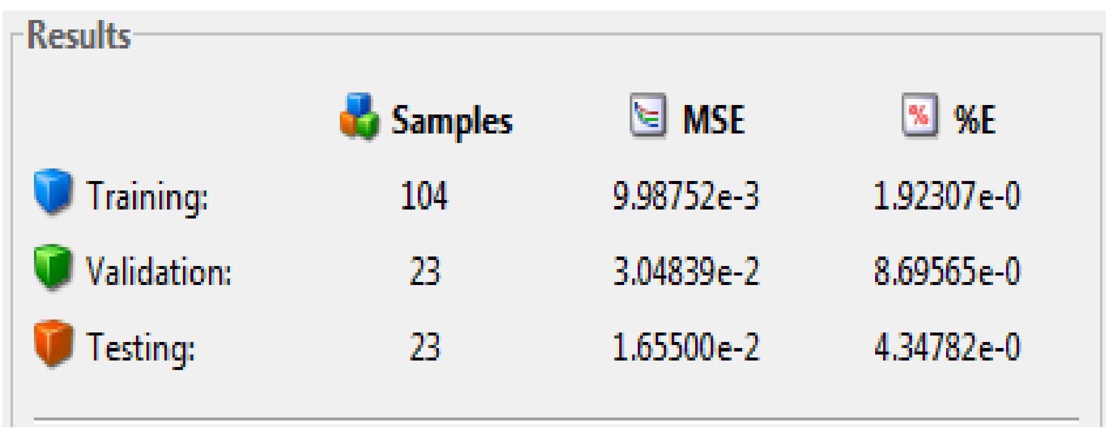

Figure 4.9. Train network diagram

After learning process was over, the performance evaluation of the network procedes to the confusion matrix. Confusion matrix expresses the correct classification and misclassification of testing data set. The Confusion matrix is used to summarize the results of a supervised classification of ANN.

Figure 4.10 shows, the number of samples correctly classified and misclassified. The diagonal element of the matrix indicates which were correctly classified and the elements below or above the diagonal elements shows the misclassified ones.

Figure 4.10. Confusion matrix of neural network

As shown in Figure 4.10, the result of artificial neural network classifier for testing using selected morphological features, from the total of 23 tested samples, 1 sample (4.3%) of fiber class was misclassified into speck class and 7 samples (30%) of fibers class, 6 samples (26.1%) of specks and 9 samples (39.1%) of masses class were correctly classified.

For training, from the total of 104 training samples, 2 samples (1.9%) of fiber were misclassified into speck class and 36 samples (34.6%) of fibers class were correctly classified and 2 samples (1.9%) of specks were misclassified into fiber class and 30 samples (28.8%) of specks class were correctly classified; From the total of 22 validation samples, 1 sample (4.5%) of fiber was misclassified into specks class and 5 samples (22.7%) of fiber class were correctly classified.

4.7. Performance Evaluation

The performance of the prediction was evaluated in terms of sensitivity, specificity and accuracy. For this model, which presented a decision of phantom image either mass, fiber or speck.

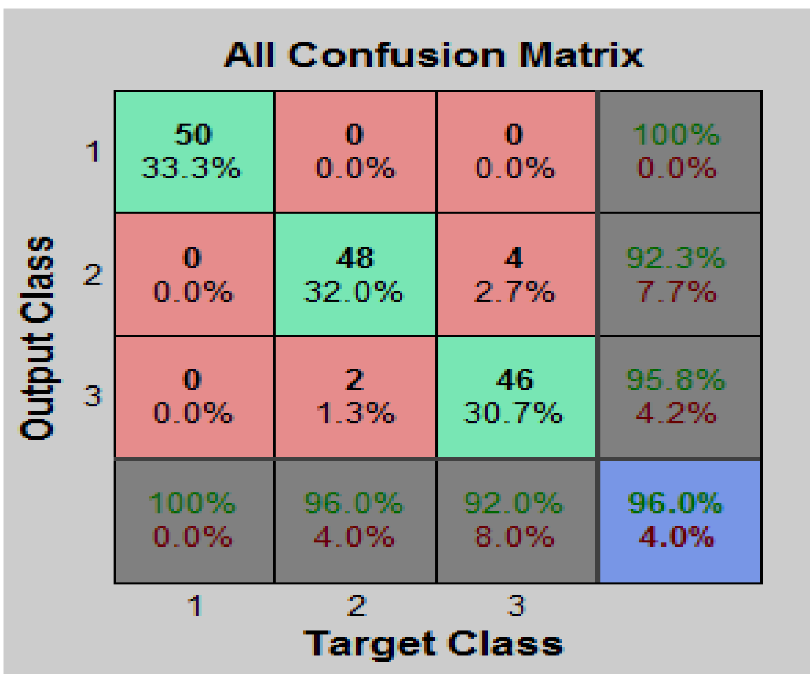

Figure 4.11. Experimental result of confusion matrix

From the confusion matrix above Figure 4.11, accuracy, sensitivity, and specificity were calculated as follows:

$$AC = \frac{TP+TN}{TP+FP+TN+FN} \times 100\% = \frac{50+48+46}{50+48+46+2+4} \times 100\% \quad (4.1)$$

$$AC = 0.96 \times 100\% = 96\% \quad (4.1a)$$

The sensitivity (referred to as the true positive rate or recall) is the probability of correctly identifying of the mass, fiber and speck given by:

$$SE = \frac{TP}{TP + FN} \times 100\% \quad (4.2)$$

$$SE = \frac{46}{46 + 2} \times 100\% = 0.95 \times 100\% = 95\% \text{ for specks} \quad (4.2a)$$

The specificity (referred to as the true negative rate) is the probability of correctly identifying is given by

$$SP = \frac{50}{48 + 4} \times 100\% = 0.925 \times 100\% = 92.5\% \quad (4.3)$$

Furthermore, for the probability of misclassification error (PME), it is obtained by

$$PME = (1 - AC) \times 100\% = 0.04 \times 100\% = 4\% \quad (4.4)$$

4.8. Comparison between Experts and Algorithm Scores

The average scores given by the radiologists for each one of features (mass, specks and fibers) in the images were compared with the corresponding scores obtained by the algorithm, the agreement between each other was good in all the compared parameters. The performance of the algorithm was defined as the total score given for each test objects. Tables (4.2 – 4.4) summarized the assessment average scores of the ACR phantom images (mass, fiber and specks) of different tube voltages as evaluated by three radiologist (for the images taken at 27kV is better for identification of the three features and followed by image at 26kV tube voltage). The Absolute percentage error of the masses, fibers and specks were determined as the ratio of the difference to expert score multiplied by one hundred.

$$\text{Absolute percentage error} = \frac{\text{Difference}}{\text{Expert Score}} \times 100\% \quad (4.5)$$

The average assessment scores given by experts, calculated by the developed algorithm for each test objects and the difference in scores given by radiologist and algorithm is summarized as follows:

Table 4.2. Comparison result of experts and algorithm average score of masses detected.

No.	Voltage Tube (kVp)	Current (mAs)	Expert Score	Algorithm Score	Difference	Absolute percentage error
1	25	92	3.67	4	-0.33	8.99%
2	26	87	4	3.67	0.33	8.25%
3	27	81	3.67	4	-0.33	8.99%
4	28	74.6	3.67	3.67	0	0
5	29	68.2	3.33	3.67	-0.34	10.2%
6	30	65	3.33	3.33	0	0%
7	31	52.9	3.33	3.67	-0.34	10.2%
8	32	54.6	3	3.33	-0.33	11%
9	33	50.3	3.33	3.33	0	0%
10	34	49.7	3	3	0	0
Total Score			34.66	35.67	1.01	2.9%

Table 4.3. Comparison result of experts and algorithm average score for fibers detected.

No.	Voltage (kv)	Current (mAs)	Expert Score	Algorithm Score	Difference	Absolute percentage error
1	25	92	3.67	4	-0.33	8.99%
2	26	87	4	3.67	0.33	8.25
3	27	81	3.67	4	0.33	8.99%
4	28	74.6	3.67	4	-0.33	8.99%
5	29	68.2	3.67	3.67	0	0
6	30	65	3.33	3.67	-0.34	10.2%
7	31	52.9	3	3.33	-0.33	11%
8	32	54.6	3	3.33	-0.33	11%
9	33	50.3	3.33	3	0.33	9.9%
10	34	49.7	3	3	0	0
Total Score			34.34	35.67	1.33	3.87%

Table 4.4. Comparison result experts and algorithm average score of specks image.

No.	Voltage (kV)	Current (mAs)	Expert Score	Algorithm Score	Difference	Absolute percentage error
1	25	92	2.33	2.67	-0.34	14.59
2	26	87	2.67	2.33	0.34	12.7
3	27	81	2.33	2.67	0.34	14.9
4	28	74.6	2.33	2.33	0	0
5	29	68.2	2.67	2.67	0	0
6	30	65	2.67	2.67	0.34	12.7
7	31	52.9	2.33	2.33	0	0
8	32	54.6	2	2.34	-0.34	17%
9	33	50.3	2.33	2.33	0.33	0
10	34	49.7	2	2	0	0
Total Score			23.66	24.34	0.68	2.87%

Table (4.2 – 4.4), shows that the number of detected artifacts by algorithm is better than the experts score. The increase in X-ray tube voltage increases the amount of radiation coming out of the X-ray tube, but the tube current exposure time product value (mAs) is decreased. The absolute percentage difference is 2.9%, 3.87%, 2.87% for mass, fiber and specks, respectively.

Figure 4.12 depicts the results for the algorithm when detecting the masses, fibers and specks, respectively compared with the evaluation of the physicians. The graph of each artifacts versus the voltage tube is summarized in Figure 4.12.

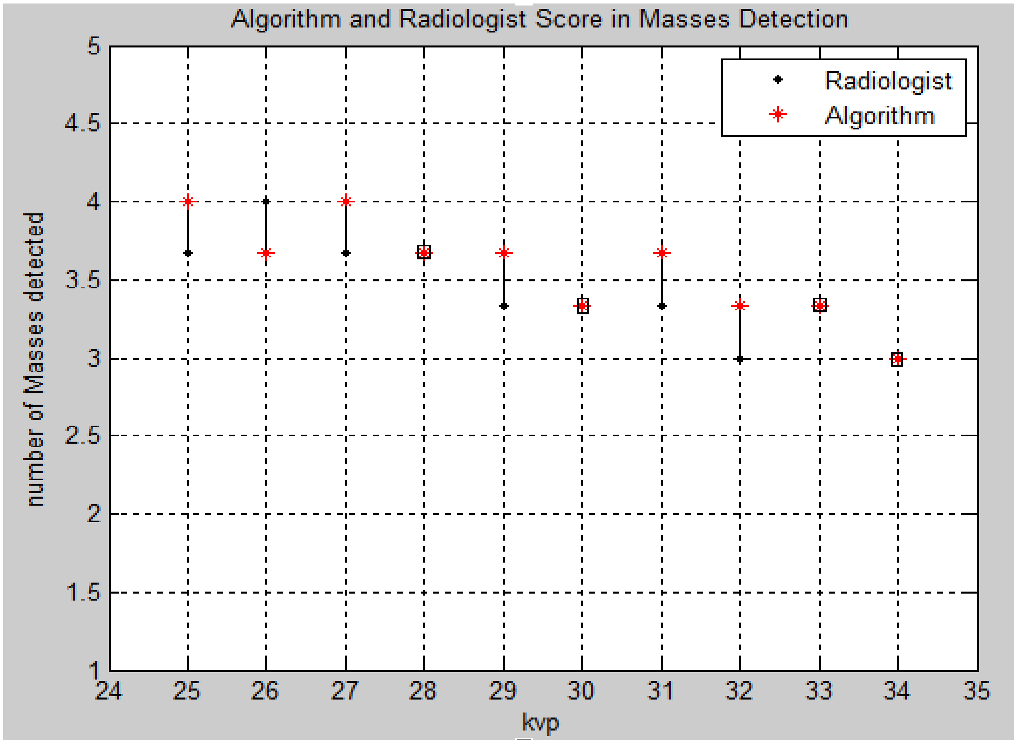
Algorithm and Radiologist Score in Masses Detection
Radiologist
Algorithm
number of Masses detected
kvp

(a)

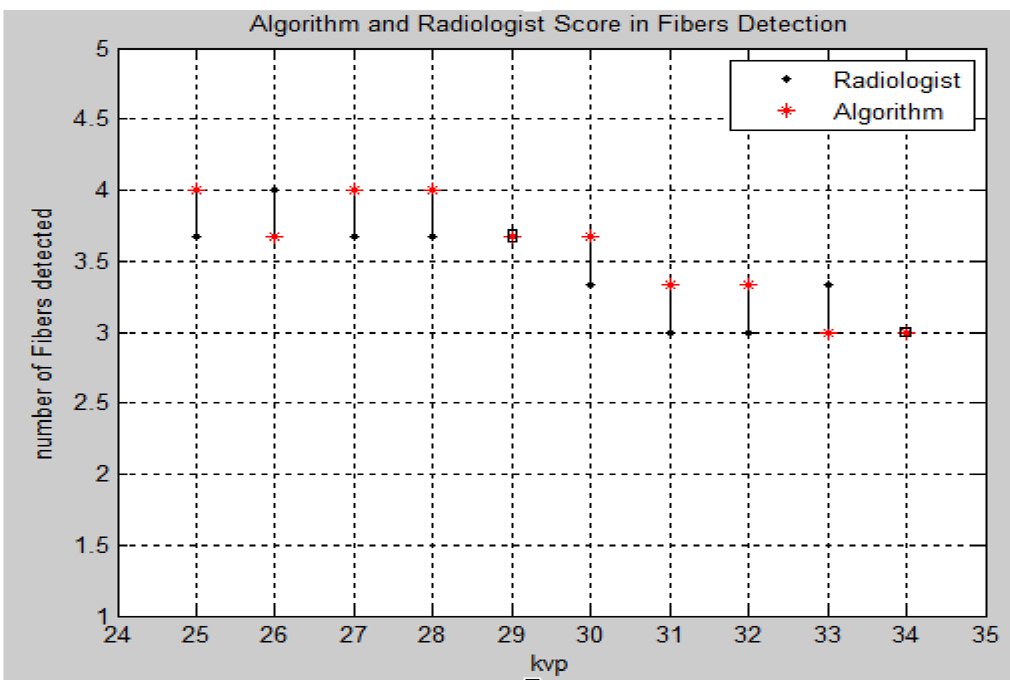
Algorithm and Radiologist Score in Fibers Detection
Radiologist
Algorithm
number of Fibers detected
kvp

(b)

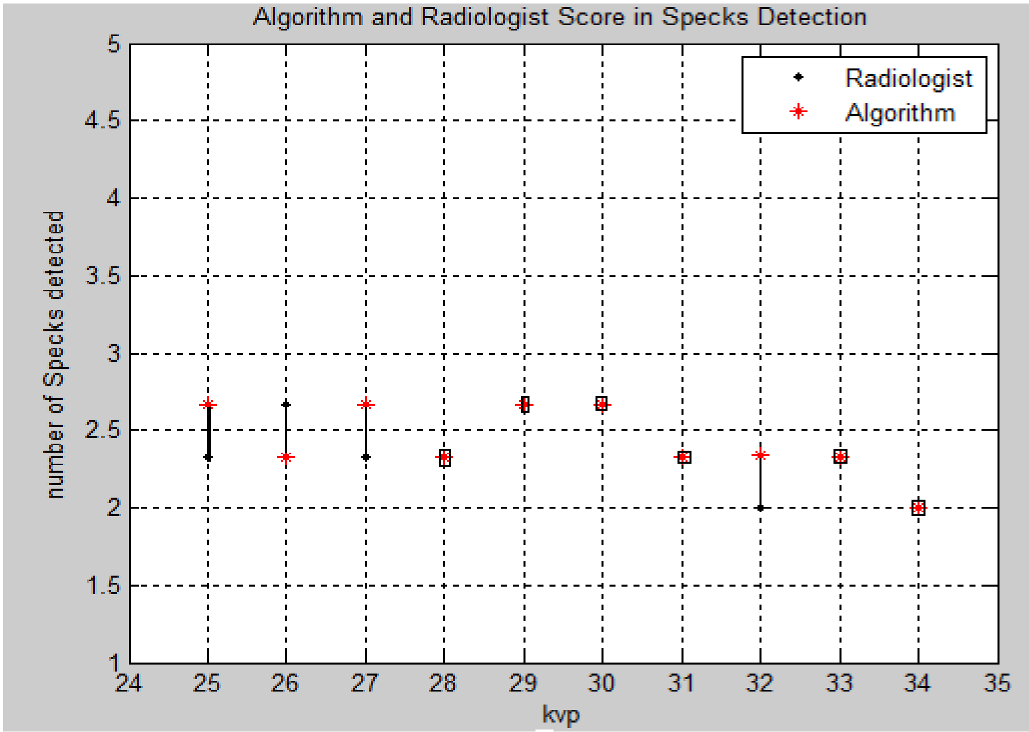

(c)

Figure 4.12. Comparison between the algorithm output and radiologists scores of artifacts of mammographic images. (a) mass's graph, (b) fiber's graph, (c) specks graph.

The graph in Figure 4.12, Shows that the number of detected artifact versus the tube voltage (kVp) of each artifact. The physicians'or experts opinion or scored is identified as ■ while the algorithm output is identified as *. The error bars defined as the difference between the algorithm and radiologist were presented in the Figures 4.12. When the physicians did not agree with each other in the number of visible test objects in the image obtained, the error bars show the deviation of the opinions.

5. SUMMARY, CONCLUSION AND RECOMMENDATIONS

5.1. Summary

This work presents a possibility of automating breast phantom scoring using image processing techniques. The ACR phantom contains clinically relevant test objects designed to represent typical breast pathologies: mass, fiber's and specks. In this work, a method has been developed to quantitatively analyze the ACR phantom images by means of automatic image processing techniques. The methods used to locate the artifacts automatically and suggests a metric for their visibility. Automatic image-processing algorithm to implement the QC process in mammographic imaging was developed. This ensured that the human observer, and the inherent variability of that observer is removed from the analysis. The visibility of the all test object groups in the phantom images obtained from various facilities have been estimated with automatic score image processing for each object. In this thesis work, the phantom image was digitalized and filtered using median filter to remove the noise. It was processed using CLAHE to increase the contrast between background and objects. Image segmentation algorithms were also implemented and evaluated using thresholding techniques to turn a gray-scale image into a binary image. The sets of extracted morphological features were used as an input to a machine learning algorithm. The artifacts (mass, fiber and speck) classification was done by artificial neural network of MATLAB toolbox which is a best classifier. The overall result of system's performance of the classifier was, 96% accuracy, 95% sensitivity and 92.5% specificity.

5.2. Conclusions

The automatic scoring provides an accurate automated measurement. It was found that as the kVp is increased, the mAs decreased, the number of visible masses, fiber and specks increased to a maximum, after which the number of visible objects decreased. Generally, based on the finding of the study and discussion above, it is possible to conclude that the mammogram of the phantom image in different kV can be classified based on features of artifacts by using morphological features. In this thesis, an artificial neural network of three layers was proposed for phatom image classification. The performance of the proposed structure were evaluated in terms of sensitivity, specificity and accuracy. Using the proposed ANN classifier, 96% accuracy, 95% sensitivity and 92.5% specificity were achieved. The implication from this is that automatic scoring of ACR phantom images is feasible and could be used as a tool to eliminate the effect of observer variability in digital mammograms. This helps radiology professionals to ensure that their mammographic system is producing images of the highest quality. These high quality images can lead to the early detection of breast cancer and long-term survival of patients. Thus, we can conclude that image processing is a non-invasive (not involving the introduction of instrument into the body) and effective tool that can be applied for classification and verification performance phantom images.

5.3. Recommendations

Breast cancer is the most common disease in women in many countries. Early detection of breast cancer can be achieved using digital mammography. However, Certain areas of research in mammography quality still require attention. For example, detection of mammography image quality using other or different phantom images phantom. It may be better if additional experiments can be performed in a larger number of phantom images obtained from different Hospitals. Further studies could also compare the different classification methods, as well as additional segmentation and enhancement techniques. Radiologist should introduce noise removal (median filter), CLAHE (image enhancement), image processing techniques knowledge, which enables them to increase or improve the visibility of artifacts (mass, fiber and specks) for early detection and classify the artifacts (mass, fiber and specks) with accurate assessment. Calibration of mammographic X-ray must follow every quality control to assure efficiency of the machine. Further study can also conducted on automatic cropping of phantom images.

6. REFERENCES

Boateng, K. O., Benjamin, W.A. and David S. L. 2012. Improving the Effectiveness of the Median Filter**.** *International Journal of Electronics and Communication Engineering*, 5(1): 85-97.

Chakraborty, D.P. 1997. Computer analysis of mammography phantom images (CAMPI): An application to the measurement of microcalcification image quality of directly acquired digital images. *Medical Physics*, *24*(8): 1269-1277.

Faulkner, K. and Law, J. 1994. A comparison of mammographic phantoms, *The British Journal of Radiology*, 67(1): 174-180.

Fausett, L. 1994. *Fundamentals of Neural Networks: Architectures, algorithms, and Application*. Prentice Hall, New Jersey Englewood Cliffs, USA.

Fischmann, A., Siegmann, K.C., Wersebe, A., Claussen, C.D. and Muller-Schimpfle, M. 2005. Comparison of full-field digital mammography and film–screen mammography: image quality and lesion detection. *The British journal of radiology*, *78*(928): 312-315.

Gong, L., Liu, C., Li, Y. and Yuan, F. 2012. Training feed-forward Neural Network Using the Gradient Descent Method with the Optimal Steps. *Journal of Computational Information System* 8(4): 1359-1371.

Gonzalez, R. C. and Woods, R. E. 2008. *Digital Image Processing*, *3rd edition*. Addison-Wesley Publishing Company, USA.

Haus, A.G., Yaffe, M.J., Feig, S.A., Hendrick, R.E., Butler, P.A., Wilcox, P.A. and Bansal, S. 2001. Relationship between phantom failure rates and radiation dose in mammography accreditation. *Medical physics*, *28*(11): 2297-2301.

Huda, W., Sajewicz, A.M., Ogden, K.M., Scalzetti, E. M. and Dance, D.R. 2002. How good is the ACR accreditation phantom for assessing image quality in digital mammography? *Academic radiology*, *9*(7): 764-772.

ICRU, 1996. Report 54 Medical imaging – the assessment of image quality, *international Commission on Radiation Units and Measurements*, *23(1): 289-292.*

Kimme-Smith, C, Bassett, L, God R. H, Fox S. A, and Solberg, T. 1992. Testing Mammography Equipments: Evolution over a 4-year period. *Med Phys*, 19(3): 1491-1494.

Laine, A., and Huda, W. 1996. Segmentation of Masses Using Continuous Scale Representations, *Proceedings of Internal Workshop on Digital Mammography Chicago*, 3(1): 447-450.

Leitz, W. K., Månsson, L.G., Hedberg-Vikström, B. R. K. and Kheddache, S. 1993. In search of optimum chest radiography techniques, *The British journal of radiology*, *66*(784): 314-321.

Mayo, P., Rodenas, F., Verdú, G., Villaescusa, J. I. and Campayo, J.M. 2004. Automatic evaluation of the image quality of a mammographic phantom. *Computer methods and programs in biomedicine*, *73*(2): 115-128.

Otsu, N. 1979.A threshold selection method from gray level histograms. *IEEE Transactions on Systems, Man and Cybernetics*, 9(1): 62-66.

Payne, M. and Lawinski, C. P. 1992. A comparison of four mammographic image quality test objects. *The British journal of radiology*, *65*(772): 339-341.

Perry, N., Broeders, M., de Wolf, C., Törnberg, S., Holland, R. and von Karsa, L. 2008. European guidelines for quality assurance in breast cancer screening and diagnosis. *Annals of Oncology*, *19*(4): 614-622.

Pradeep N., Girisha H., Sreepathi B.,and Karibasappa K. 2012. Feature Extraction of Mammograms *International Journal of Bioinformatics Research* 4(1):241-244.

Semarya Berhe Lemlem, Worknish Sinishaw, Mignote Hailu, Mesfin Abebe, and Alemseged Aregay. 2011. Assessment of Knowledge of Breast Cancer and Screening Methods among Nurses in University Hospitals in Addis Ababa, Ethiopia.1-11.

Sharma, D. P. 2013. Intensity transformation using contrast limited adaptive histogram equalization. *International Journal of Engineering Research*, *2*(4): 282-285.

Solomon, C. and Breckon, T. 2010. Fundamentals of Digital Image processing. *A Practical Approach with Examples in MATLAB*, John Wiley and sons, West Sussex, P.O. 198SQ, UK.

Vaidehi, K. and Subashini, T. S. 2012. A global approach for detecting mass in Digital Mammograms. *International Journal of Advancements in Research and Technology*, *1*(6): 1-4.

Vala, M. H. J. and Baxi, A. 2013. A review on Otsu image segmentation algorithm. *International Journal of Advanced Research in Computer Engineering and Technology (IJARCET)*, *2*(2): 387-389.

Verma, B. and Zhang, P. 2007. A Novel Neural-Genetic Algorithm to Find the Most Significant Combination of Features in Digital Mammograms, Applied Soft Computing, 7(1): 513-525.

Wagner, R. F., Beiden, S. V., Campbell, G., Metz, C.E., Jiang, Y. and Chan, H.P. 2001. Multiple-reader studies, digital mammography, computer-aided diagnosis, and the Holy Grail of imaging physics. *Physics of Medical Imaging* , 2(420): 619-626.

7. APPENDICES

Appendix I

1. MATLAB Function and codes

Appendix i (a).Median filter MATLAB code

```
% median filter
clc; % Clear command window.
clear; % Delete all variables.
close all; % Close all figure windows except those created by imtool.
workspace;  % Make sure the workspace panel is showing.
I=imread('binarized s.png');
figure,imshow(I)
I1=medfilt2(I,[3 3]); %Apply to original image
imshow(I1)
% Median filter
% Here we define a 3x3 median filtermedfilt2()and apply it to the three
images generated
I2=medfilt2(I1,[3 3]); %Apply to salt and pepper image
I3=medfilt2(I2,[3 3]); %Apply to Gaussian image
subplot(1,3,1), imshow(I1); %Display result image
subplot(1,3,2), imshow(I2); %Display result image
subplot(1,3,3), imshow(I3); %Display result imag
```

Appendix i (b). MATLAB code Binarizing Phantom Images

```
clc; % Clear command window.
clear; % Delete all variables.
close all; % Close all figure windows except those created by imtool.
[fname, path]=uigetfile('*.pgm');
myimage=imread('Fl.png');
mycolorimage=imresize(myimage,[256,256],'nearest');
mygrayimage=rgb2gray(mycolorimage);
mybwimage=im2bw(mycolorimage);
subplot(2,2,1);
imshow(mycolorimage);title('Fl Orginal image')
subplot(2,2,2);
imshow(mybwimage);title('Fl binary image');
imwrite(mybwimage,'binarized Fl.png');
```

Appendix i (c). Small area Removal MATLAB code

```
clc; % Clear command window.
clear; % Delete all variables.
close all; % Close all figure windows except those created by imtool.
[fname, path]=uigetfile('*.pgm');
I=imread(strcat(path,fname));%read the orginal image
BW = im2bw(I, .05);%thresholding the orginal image usin T=13.
%Determine the connected components:
conn=8;%default vaue
CC = bwconncomp(BW, conn);
%Compute the area of each component:
S = regionprops(CC, 'Area');
L = labelmatrix(CC);%label each area
```

```
BW3 = bwareaopen(L, 1);%Remove small area objects:
se = strel('disk',5);%structural element with flat disk shape and radius=5
im1=imerode(BW3,se);%erode the image
im2=imdilate(im1,se);%dilat the image
im3 = imfill(im2,'holes');%fill holes if there
K=immultiply(im3,I);%multiply the orginal image with binary image of
the breast area
figure,imshow(K)
B = medfilt2(K, [3 3]);%median filter to reduce noise,lines and preserve
edges.
imwrite(B,'filename.jpg');
```

Appendix i (d). Enhancement MATLAB code

```
% for binarized image
clc; % Clear command window.
clear; % Delete all variables.
close all; % Close all figure windows except those created by imtool.
[fname, path]=uigetfile('*.pgm');
grayImage=imread(strcat(path,fname));
figure, subplot(2,2,1),imshow(grayImage);title('orginal image');
A = adapthisteq(grayImage,'clipLimit',0.01,'Distribution','uniform');
B = adapthisteq(grayImage,'clipLimit',0.01,'Distribution','exponential');
C = adapthisteq(grayImage,'clipLimit',0.01,'Distribution','rayleigh');
subplot(2,2,2),imshow(A),title('CLAHE with uniform Distribution');
subplot(2,2,3),imshow(B),title('CLAHE with exponetial Distribution');
subplot(2,2,4),imshow(C),title('CLAHE with rayleigh Distribution');
imwrite(A,'m11.pgm');
```

Appendix i (e). MATLAB code for Segmentation using Thresholding

```
clc; % Clear command window.
clear; % Delete all variables.
close all; % Close all figure windows except those created by imtool.
a=imread('Fr.png');
level=graythresh(a);
c=im2bw(a,level);
subplot(1,2,1), imshow(a),title('Orginal image');
subplot(1,2,2), imshow(c),title('thresholding out');
imwrite(c,'Fr.JPG');
```

Appendix i (f). Morphological Feature extraction MATLAB code

```
%Use binarized image
clc; % Clear command window.
clear; % Delete all variables.
close all; % Close all figure windows except those created by
imtool.I=imread('binarized Fl.png');
%I=rgb2gray(I);
%I2=thresholding(I);
imshow(I);
cc=bwconncomp(I,8);
n=cc.NumObjects;
Area=zeros(n,1);
Perimeter=zeros(n,1);
MajorAxis=zeros(n,1);
```

```
MinorAxis=zeros(n,1);
k=regionprops(I,'Area','Perimeter','MajorAxisLength','MinorAxisLength');
for i=1:n
        Area=cat(i, k.Area);
        Perimeter=cat(i,k.Perimeter);
        MajorAxis=cat(i,k.MajorAxisLength);
        MinorAxis=cat(i,k.MinorAxisLength);
        Elongation=MajorAxis./MinorAxis;

End
```

Appendix i (g). Plotting graph MATLAB code

```
clear all
close all
fontsize=20;
x=[25 26 27 28 29 30 31 32 33 34];% voltage tube parameter
y1=[2.33 2.67 2.67 2.33 2.67 2.67 2.33 2 2.33 2];% Radiologist score
y2=[2.33 2.33 2.33 2.67 2.67 2.33 2.33 2.34 2 2];% Algorithm score
 xlabel('Number of '),ylabel('Number of Specks Detected ')
%err = [0.1 0.1 0.1 0.1];
%errorbar(x,y1,err,'.b')
figure,plot(x,y1,'.k',x,y2,'*r');
% Add a legend
title('Algorithm and Radiologist Score in Specks Detection')
xlabel('kvp'),ylabel('number of Specks detected')
legend('Radiologist','Algorithm')
axis([24 35 1 5])
grid on
box on
```

Appendix i (h). ANN classification MATLAB code

```
clear; % Delete all variables.
close all; % Close all figure windows except those created by imtool.
Inputs = [1494 1.745, 1046   1.124; 2282 1.549, 2046 1.549; 2412 0.645,
2373 0.523];
simpleclassInputs=Inputs';
Targets = [1 0 0 ;0 1 0;0 0 1];
simpleclassTargets= Targets';
b=Targets;
disp(simpleclassInputs);
disp(simpleclassTargets);
net = newpr(simpleclassInputs,simpleclassTargets,20);
net = train(net,simpleclassInputs,simpleclassTargets);
simpleclassOutputs = sim(net,simpleclassInputs);
plotconfusion(simpleclassTargets,simpleclassOutputs);
if ('b==[0 0 1]');
disp('Mass');
elseif (b==[0 1 0]')
disp('Fiber');
elseif (b==[0 0 1]');
disp('speck');
else
disp('error');
end
```

Appendix II

Appendix II Figure 7.1. Original phantom images of Kad1

Ff k1 Ffk2 Ffk3 Ffk4

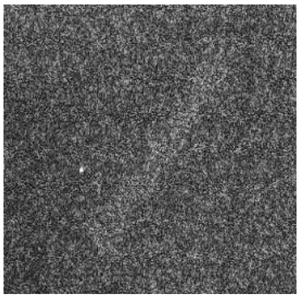
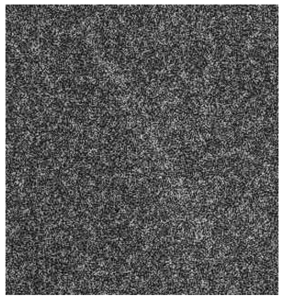
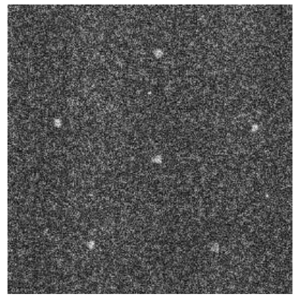
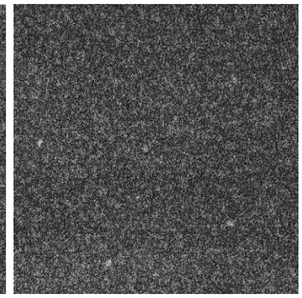

Ffk5 Ffk6

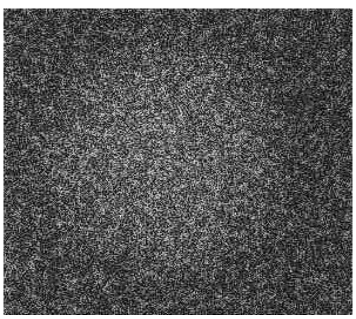
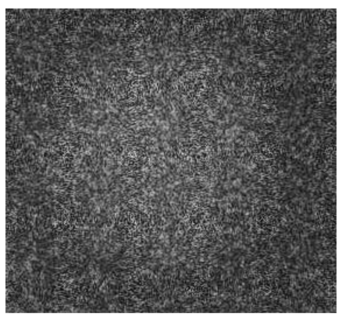

Appendix II figure 7.2.Original Phantom image of Kad2

Ff k21 Ffk22 Ffk23 Ffk24

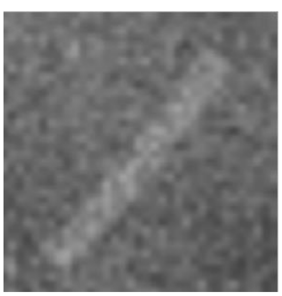
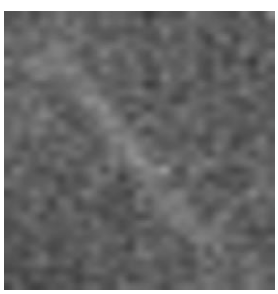
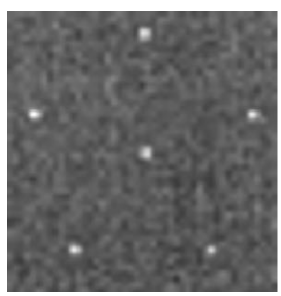
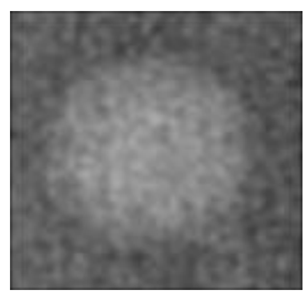

Ff k29 Ffk221 Ffk222 Ffk223

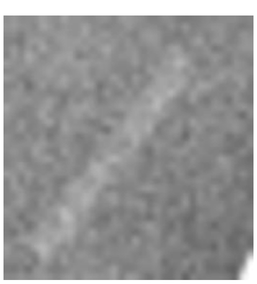
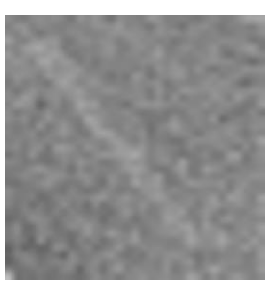
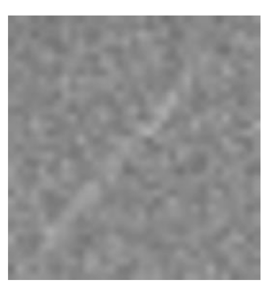
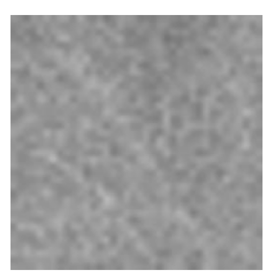

Ffk224

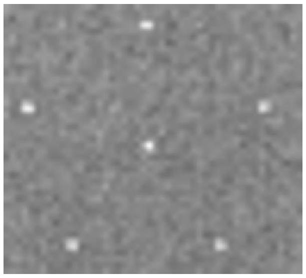

Ffk225

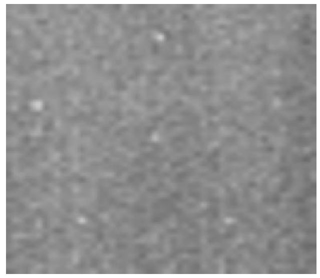

Appendix II figure 7.3. Original Phantom image of kad3.

Ff k31

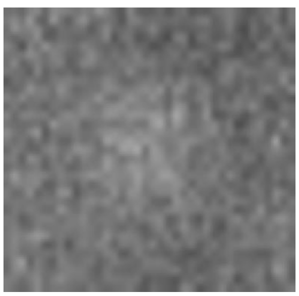

Ffk32

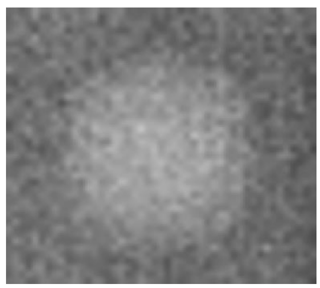

Ffk33

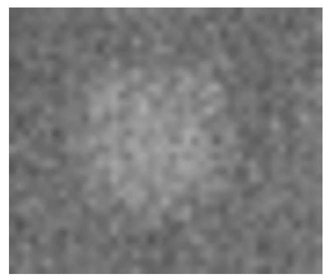

Ff k34

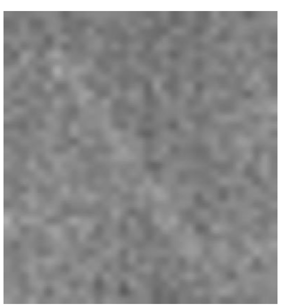

Ffk35

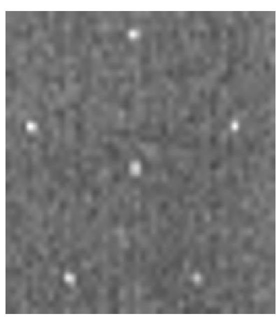

Ffk36

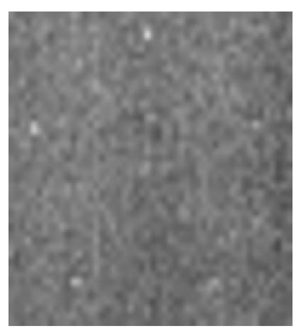

Ffk37

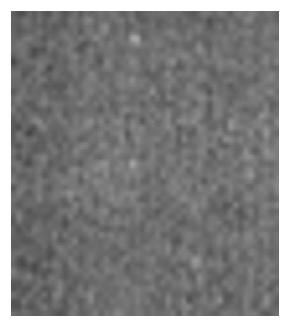

Ff k38

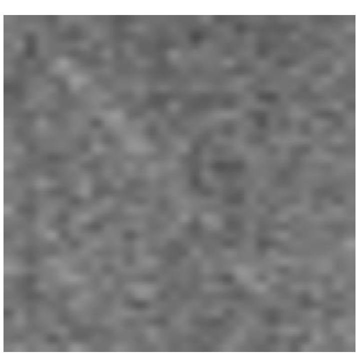

Ffk39

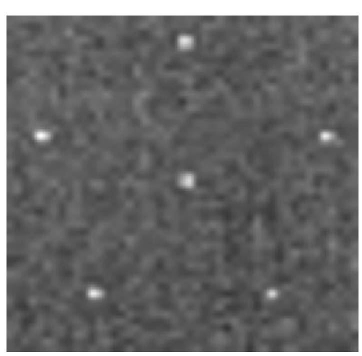

Ffk331

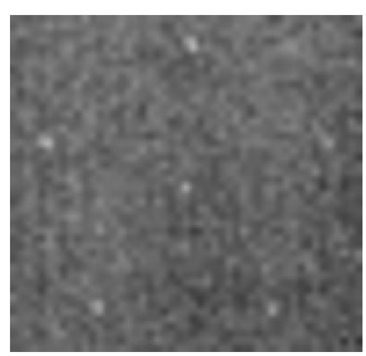

Ffk332 Ffk333 Ffk334

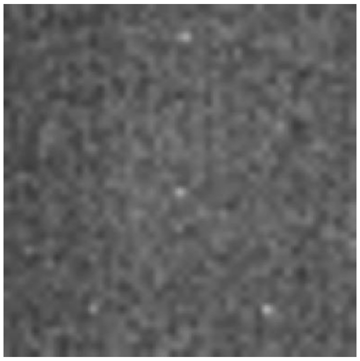
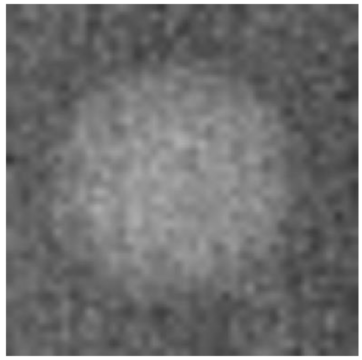
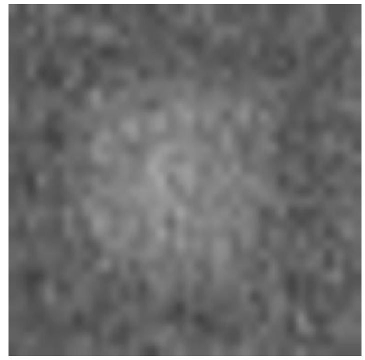

Appendix figure 7.4. Original Phantom image of Kad4

Ffk41 Ffk42 Ffk43

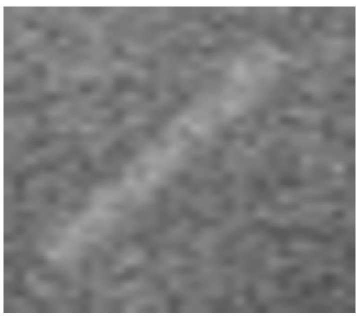
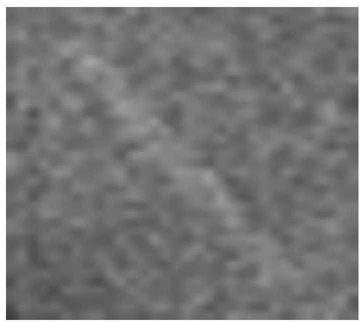
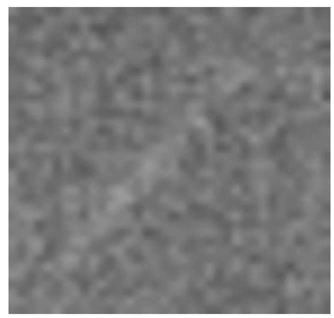

Ffk44 Ffk45 Ffk46

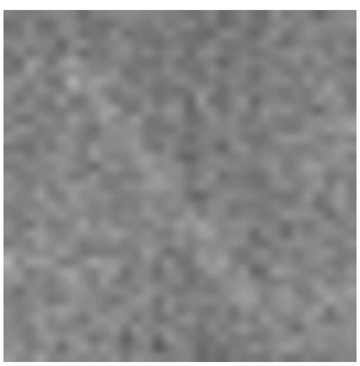
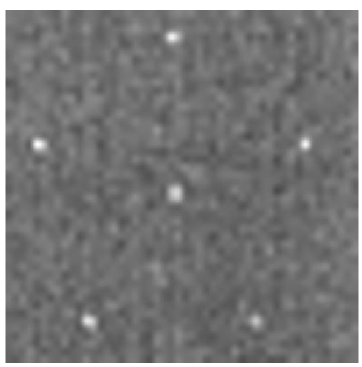


Ffk47 Ffk48 Ffk49

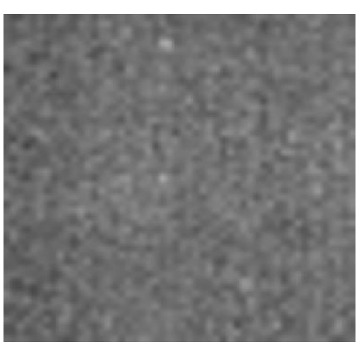
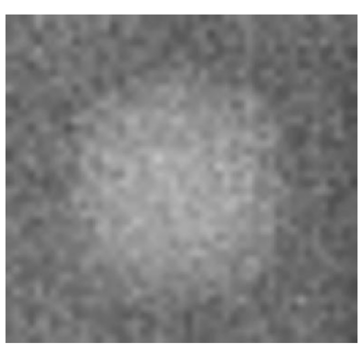
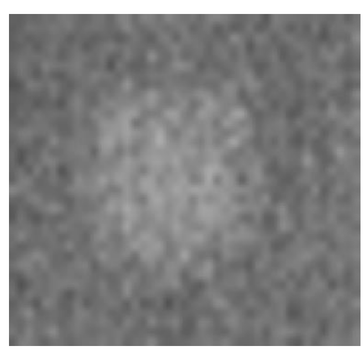

Appendix figure 7.5. Original Phantom image of Kad5

Ffk51

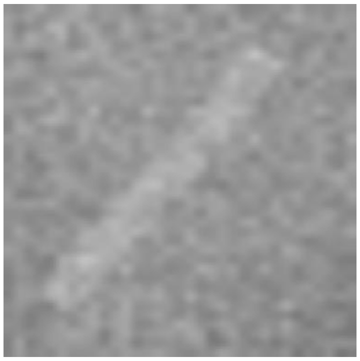

Ffk52

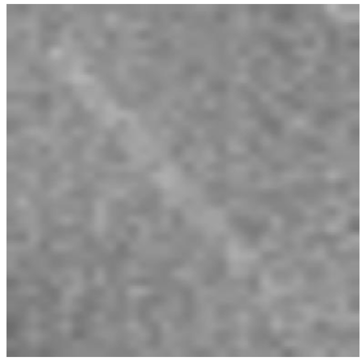

Ffk53

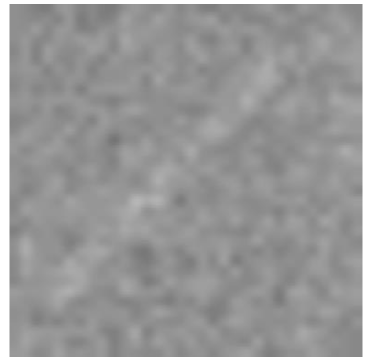

Ffk54

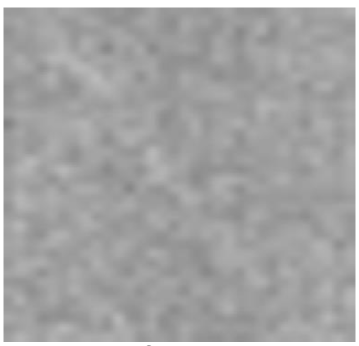

Ffk55

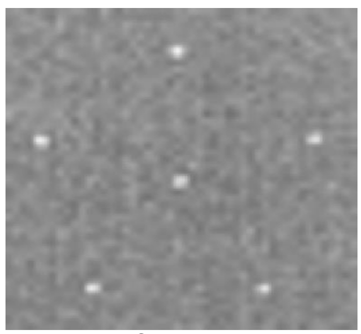

Ffk56

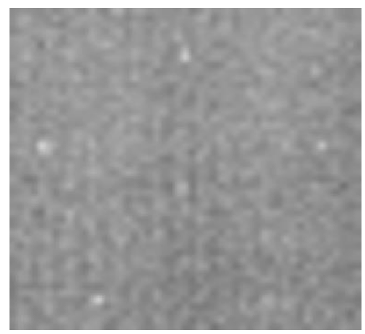

Ffk57

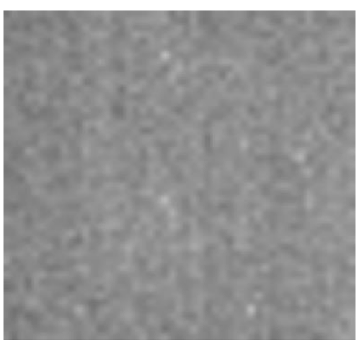

Ffk58

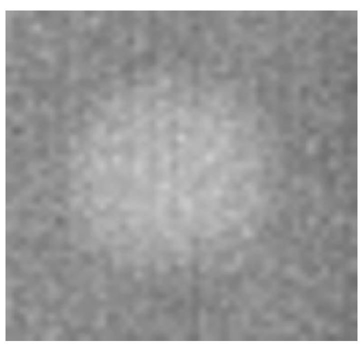

Ffk59

Appendix figure 7.6. Original Phantom image of kad6

Ffk61

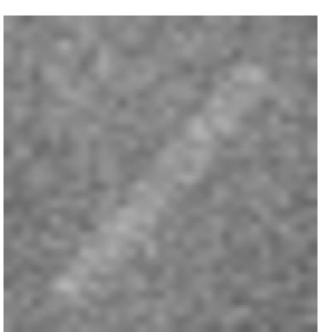

Ffk62

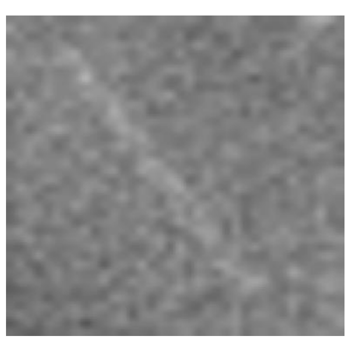

Ffk63

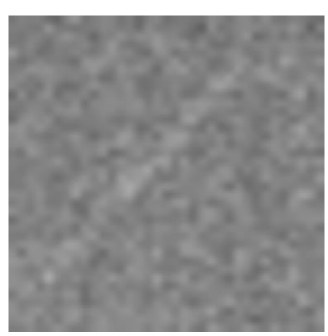

Ffk64

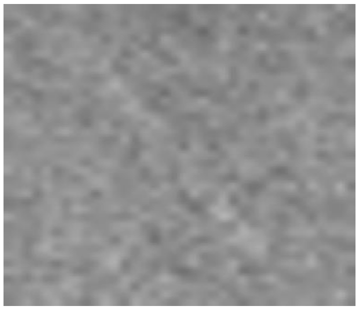

Ffk65

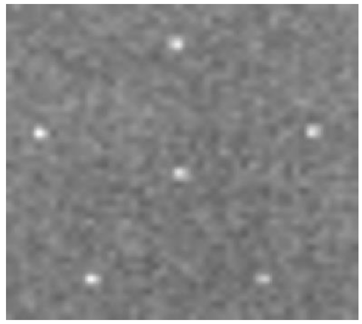

Ffk66

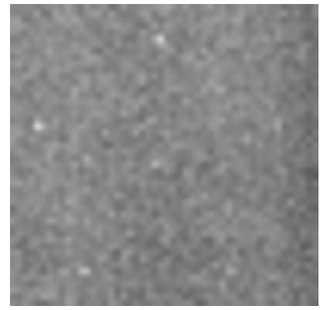

Ffk67

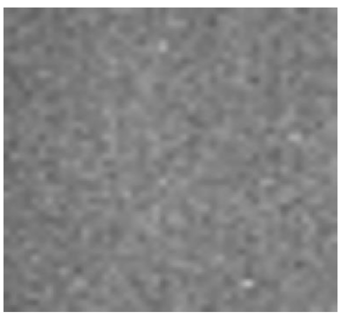

Ffk68

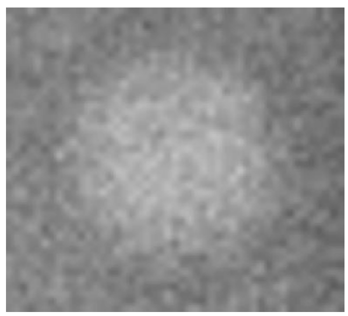

Ffk69

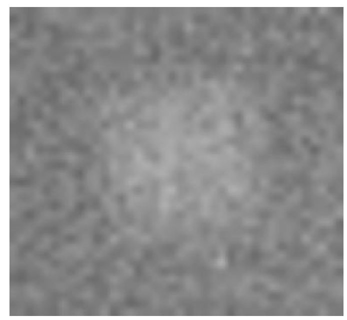

Appendix figure 7.7. Original Phantom image of Kad7

Ffk71

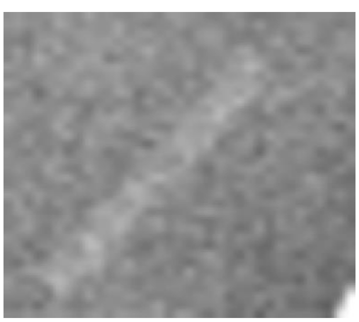

Ffk72

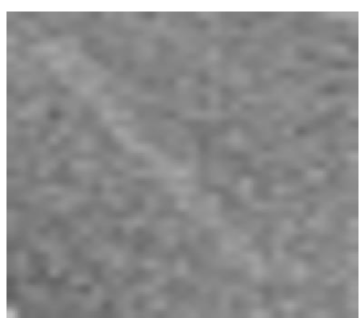

Ffk73

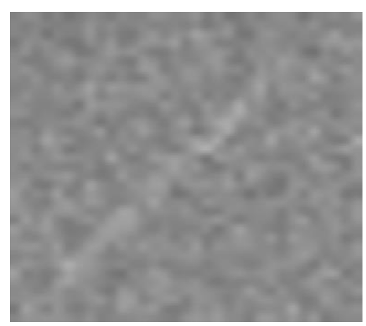

Ffk74

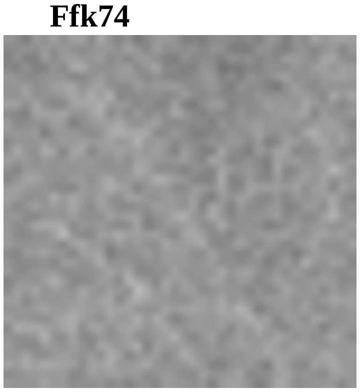

Ffk75

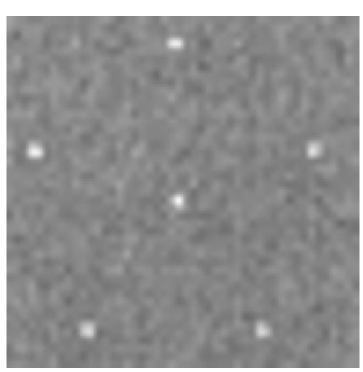

Ffk76

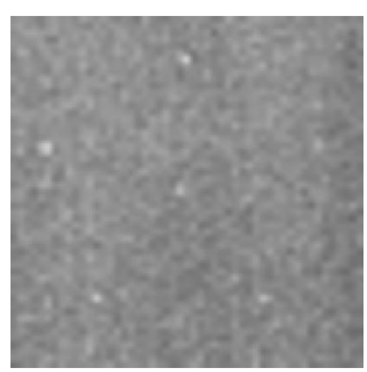

Ffk77

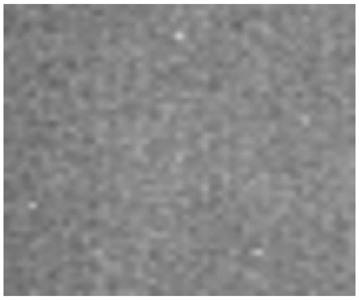

Ffk78

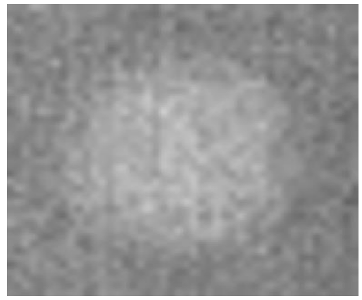

Ffk79

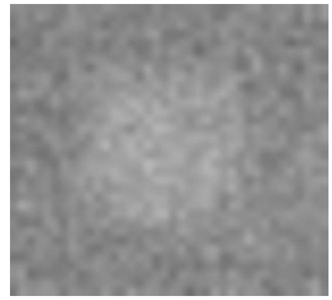

Ffk771

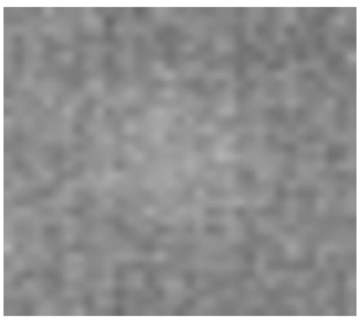

Appendix III

Appendix V figure 4 .ANN train

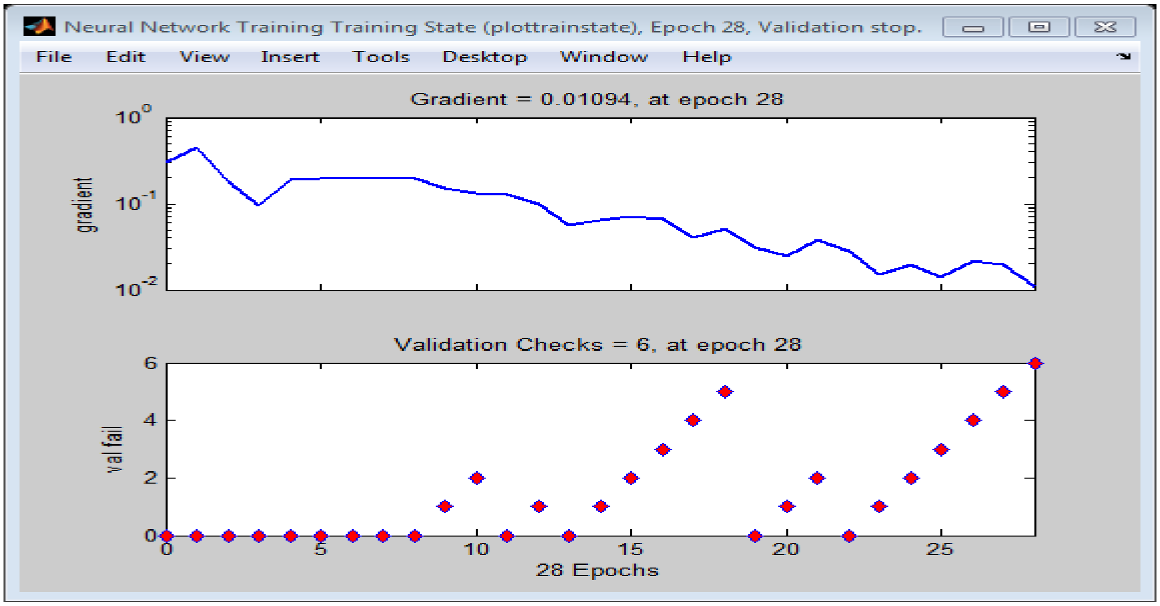

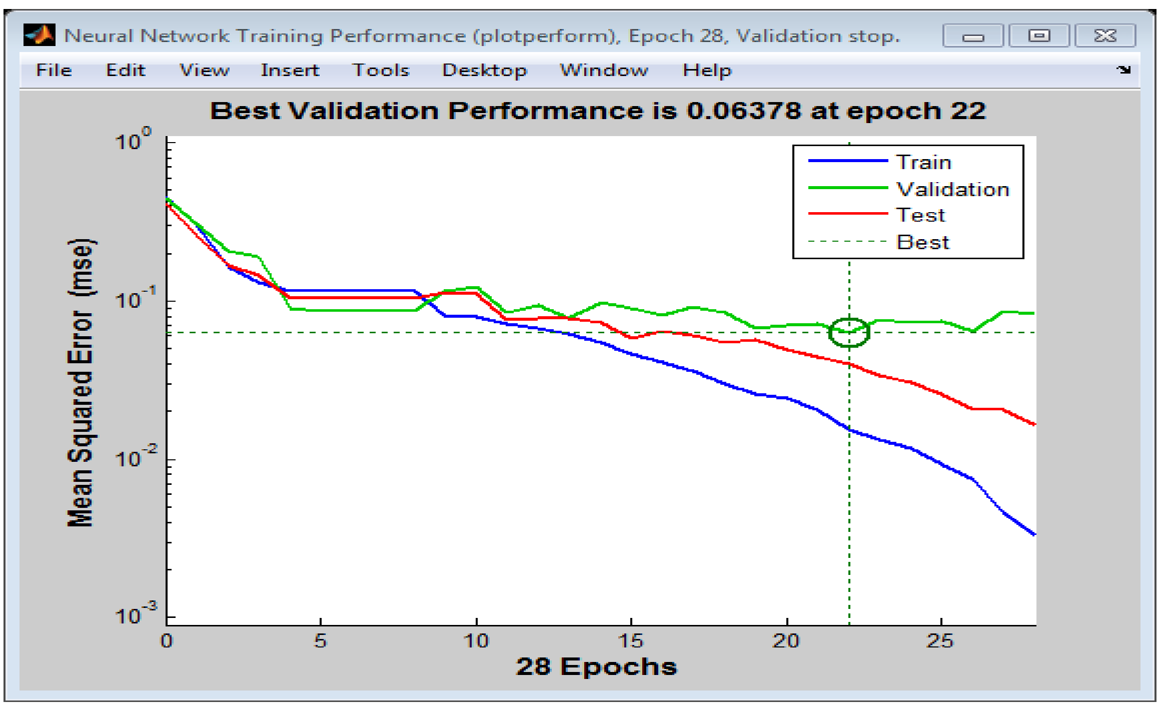

Figure 2. Best validation performance

Appendix IV

Appendix Table 1. Morphological feature extracted from the Phantom images (fibers).

Objects	Area	Major axis	Minor axis	Perimeter	Aspect ratio	Circularity
F11	846	348.12	234.73	8.24	1.48	58.00
F12	264	262.71	158.48	43.69	1.65	26.00
F13	123	193	128.1	52	1.5	52.00
F14	324	346.74	227.16	37.5	1.52	38.00
F15	354	276.67	158.39	56.62	1.75	46.00
F16	424	346.83	237	48.5	1.46	42.23
F17	362	264.64	146.36	56.62	1.8	35.00
F18	346	314.32	231.23	8.24	1.35	31.00
F19	301	189.15	132.15	47.36	1.43	44.00
F20	101	212	163	52	1.5	45.00
F21	471	177.11	122.1	48.34	1.45	43.10
F21	423	186.12	132.65	54.37	1.4	33.51
F22	352	232.12	163.02	67	1.55	39.21
F22	445	271.37	163.02	52.26	1.66	1.51
F23	523	287.08	172.42	45.39	1.66	23.00
F24	416	184.81	112.46	55.43	165	42.03

Appendix Table 2. Morphological feature extracted from the Phantom images (masses).

Objects	Area	Major axis	Minor axis	Perimeter	Aspect ratio	Circularity
M12	278	363.32	323.64	20.83	1.04	1.32
M13	798	356.17	337.43	23.4	1.05	1.19
M14	273	365.35	358.43	64.03	1.17	1.43
M15	423	445.23	433	53.92	1.02	1.26
M16	286	340.32	323.41	64.03	1.05	1.32
M17	439	425.2	413.21	47.53	1.03	1.06
M18	673	336.14	315.4	23.4	1.07	1.26
M19	586	423.95	397	26.73	1.07	2.47
M20	276	262.71	127.14	43.69	0.98	1.56
M21	269	345.71	332.74	26.82	1.04	1.35
M22	367	287.65	235.32	2.14	1.22	1.19
M22	376	277.65	246.67	37.42	1.12	1.23
M22	465	384.26	234.41	2.14	1.64	1.27
M22	364	242.21	165.25	62	1.46	35.31
M22	376	276.54	236.56	36.42	1.17	1.14
M23	476	280.6	165.03	41.56	1.7	1.45
M23	387	362.31	279.45	57.63	1.29	1.68
M24	389	363.7	350.73	49.82	1.4	1.43
M24	379	371.61	262	69.25	1.42	1.46
M24	374	253.12	176.32	56.23	1.43	1.31

Appendix Table 3. Morphological feature extracted from the Phantom images (specks).

Objects	Area	Major axis	Minor axis	Perimeter	Aspect ratio	Circularity
S11	314	321.98	317.07	65.49	1.02	1.32
S12	342	238.54	246	2.14	0.97	1.21
S13	322	182.11	154.19	47.36	1.18	49
S14	645	115.21	115.13	124	1	1.15
S15	361	264.63	335.05	214	0.79	1.08
S16	432	435.23	433.24	45.6	1	1.06
S17	321	246.83	254.08	63	0.97	1.02
S18	598	364.17	349.32	32.64	0.99	1.13
S19	421	234.9	232.05	68	0.99	1.12
S20	346	348.61	298.13	65.49	1.16	1.06
S21	333	257.56	316.05	2.14	0.523	0.98
S22	642	215.04	216.02	2.83	1	1.06
S22	664	265.03	266.04	46.53	1.08	1.06
S22	635	274.13	256.24	48.32	1.07	1.09
S23	432	168.23	134.47	63.02	1.25	1.23
S24	541	272.34	263.71	46.92	1.03	1.02
S25	367	277.65	265.05	2.14	1.05	0.97